JOURNAL OF PETROLOGY | VOLUME 41 | NUMBER 3 | PAGES 387–409 | 2000

Chromite in Komatiites, II. Modification during Greenschist to Mid-Amphibolite Facies Metamorphism

STEPHEN J. BARNES

CSIRO EXPLORATION AND MINING, PRIVATE BAG, WEMBLEY, WA 6014, AUSTRALIA

RECEIVED OCTOBER 25, 1998; REVISED TYPESCRIPT ACCEPTED SEPTEMBER 2, 1999

Chromite compositions in komatiites are influenced by metamorphic processes, particularly above 500°C. Metamorphosed chromite is substantially more iron rich than igneous precursors, as a result of Mg–Fe exchange with silicates and carbonates. Chromite metamorphosed to amphibolite facies is enriched in Zn and Fe, and depleted in Ni, relative to lower metamorphic grades. Relative proportions of the trivalent ions Cr^{3+}, Al^{3+} and Fe^{3+} are not greatly modified by metamorphism up to lower amphibolite facies, although minor Fe^{3+} depletion occurs during talc–carbonate alteration at low temperature. Significant Al is lost from chromite cores above 550°C, as a result of equilibration with fluids in equilibrium with chlorite. Elevated Zn content in chromite is restricted to rocks with low (metamorphic) Mg/Fe ratios, and is the result of introduction of Zn during low-temperature alteration, with further concentration and homogenization during prograde metamorphism. Cobalt and Mn also behave similarly, except where carbonate minerals are predominant in the metamorphic assemblage. Chromite at amphibolite facies is typically extensively replaced by magnetite. This is the result of incomplete metamorphic reaction between chromite and chlorite-bearing silicate assemblages. Magnetite compositions at the inner chromite–magnetite boundary are indicators of metamorphic grade.

KEY WORDS: *chromite; komatiite; spinel; metamorphism; Zn*

INTRODUCTION

Chromite in komatiites at low metamorphic grades can be a useful indicator of crystallization environment, as described in Part 1 of this series (Barnes, 1998). However, chromite is highly susceptible to modification during early hydrous alteration and subsequent prograde metamorphism of host rocks. This modification is the subject of this paper.

Metamorphic modification of chromite has been discussed extensively in the literature in the context mainly of ophiolitic or 'alpine ultramafic' complexes (Onyeagocha, 1974; Ulmer, 1974; Evans & Frost, 1975; Hoffman & Walker, 1978; Loferski & Lipin, 1983; Kimball, 1990; Burkhard, 1993) and in a few studies of komatiitic rocks (Bliss & MacLean, 1975; Donaldson, 1983; Gole & Hill, 1990), and in a detailed study of the Pechenga intrusions (Abzalov, 1998). These studies have highlighted two important effects. First, chromites become rimmed and progressively replaced by chromian magnetite or 'ferritchromit'. Second, chromite core compositions become progressively modified during prograde metamorphism as a result of exchange of components with surrounding silicate minerals (Evans & Frost, 1975; Abzalov, 1998). This paper examines the nature and magnitude of these effects in komatiites from a variety of localities in the Eastern Goldfields Province of the Archaean Yilgarn Block in Western Australia (Fig. 1). Brief locality descriptions are given in Appendix B.

PETROGRAPHIC FEATURES OF KOMATIITIC CHROMITE

It is clear from petrographic observations that alteration and metamorphism have profound effects on spinel in all but the freshest, least altered komatiites (Fig. 2).

*E-mail: barnes.s@per.dem.csiro.au

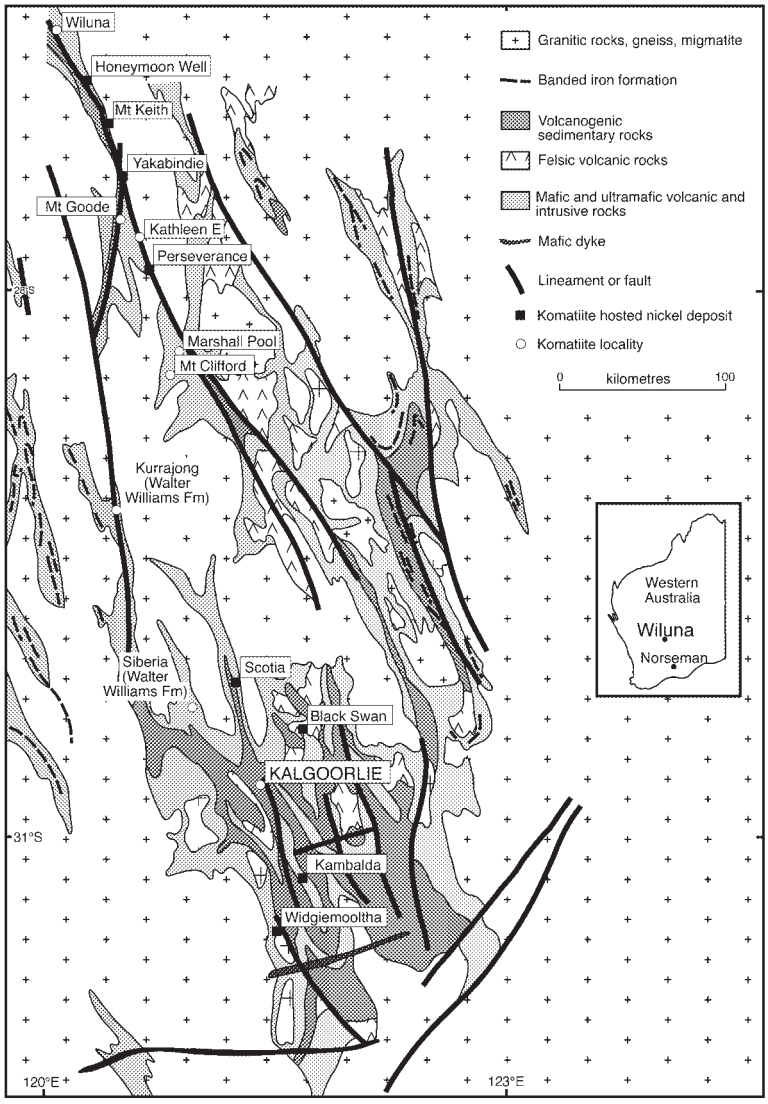

Fig. 1. Location map of Norseman–Wiluna Greenstone Belt showing localities mentioned in the text.

Chromian spinel in komatiites at low metamorphic grades is chromite and magnesiochromite, typically with euhedral cubic morphologies, and often associated with coatings and thin rims of magnetite derived from serpentinization of olivine in the host rock. Magnetite typically forms ragged coatings overgrown onto the primary growth faces of the chromite (Fig. 2a–c), and penetrating as fillings along open fractures. With more extensive fluid interaction, narrow alteration zones develop around the margins and fracture rims of the chromite in contact with the magnetite, these rims being defined by diffusive replacement of Mg^{2+} by Fe^{2+} in the spinel structure (resulting in higher average mass number, or lighter shades on the electron micrographs). Chromite with magnetite overgrowth, where original chromite grain boundaries are clearly visible, is referred to as 'type 1 spinel'.

Around the greenschist–amphibolite transition, the chromite–magnetite relationship changes to that depicted in Fig. 2f–h. Rather than forming overgrowths on euhedral chromite cores, magnetite occurs as replacement of the original chromite core. The internal chromite–magnetite boundary, rather than being the original chromite crystal growth face, now becomes a sharp, curved and lobate phase boundary between the two coexisting phases. This magnetite rim is typically concentrically zoned, as discussed in detail below. These composite grains are referred to as 'type 2 spinels'. The proportion of magnetite appears to increase with increasing metamorphic grade. In mid-amphibolite facies areas, such as Perseverance,

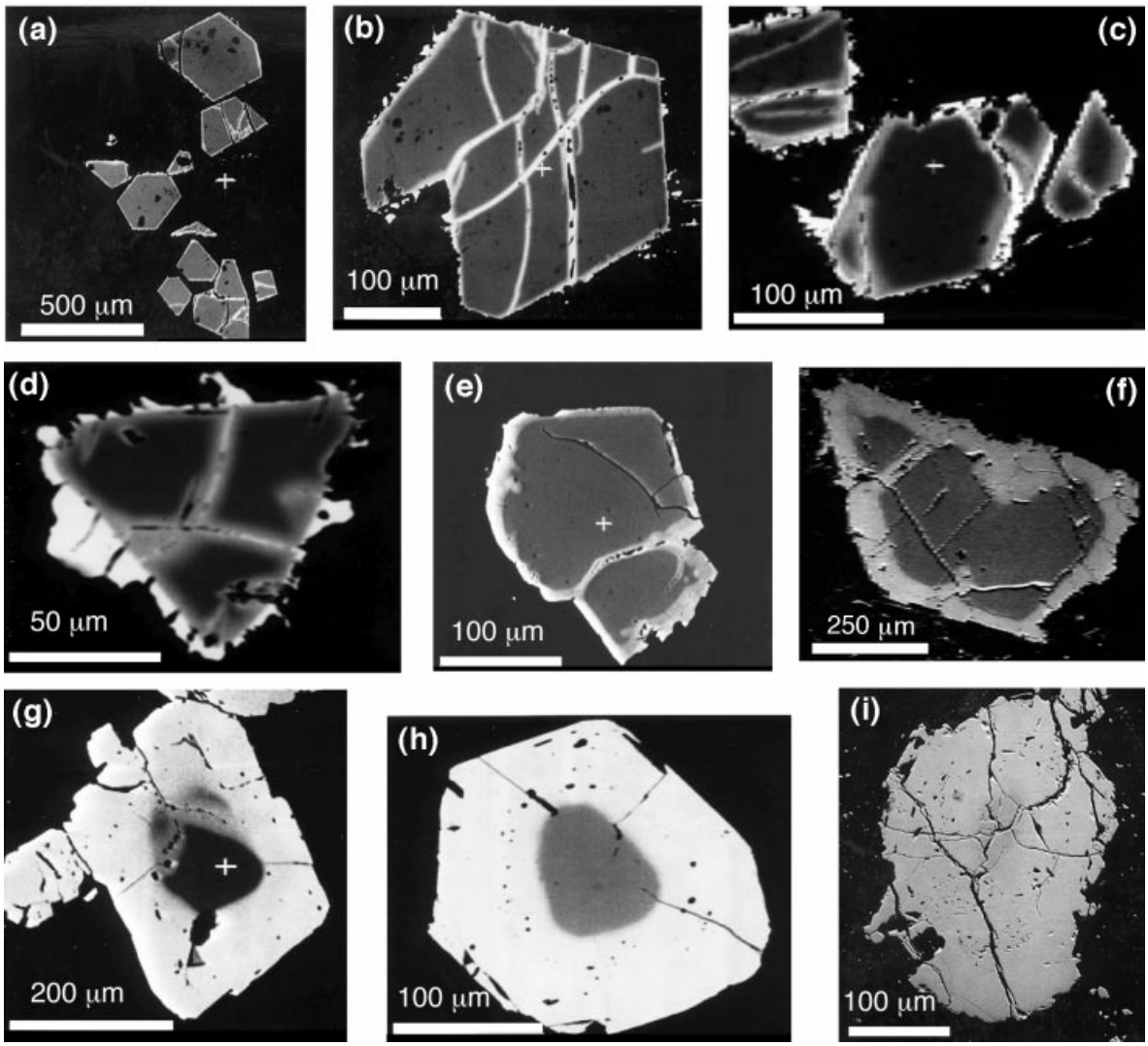

Fig. 2. Back-scattered electron micrographs of chromites and composite chromite–chromian magnetite grains, illustrating progressive replacement of chromite by magnetite during progressive metamorphism. (a) Pristine euhedral igneous magnesiochromite, no magnetite. (b) Igneous magnesiochromite, euhedral outline, with thin magnetite overgrowth and incipient penetration of magnetite along fractures. (c)–(e) More advanced magnetite veining, and development of diffuse Fe-rich chromite rinds on magnetite veins and rims. Magnetite still forms ragged non-idiomorphic grain boundaries against enclosing silicates. Samples (a)–(e) from lower greenschist facies, Mt Keith, Western Australia. (f) Incipient development of outer crystal faces on magnetite rim, and sharp, lobate internal phase boundaries against chromite. Magnetite rim is zoned from Cr bearing at inner contact to Cr free at outer margin. From upper greenschist facies area, Walter Williams Formation, Siberia. (g), (h) Advanced replacement of chromite by zoned chromian magnetite. Inner boundary is a sharp phase boundary. Annular zone of pits in photo may mark original boundary of chromite. From mid-amphibolite facies, Windarra, Western Australia. (i) Almost complete replacement. Inner, slightly darker zone is chromian magnetite. Also contains annular zone of inclusions marking original chromite grain boundary. Chromite cores have almost completely disappeared in this sample. From Digger Rocks, Forrestania. Photos (a)–(d) are referred to as 'type 1' chromite grains, photos (f)–(i) as 'type 2' composite chromite–magnetite grains.

chromite grains are almost completely replaced by magnetite and chromite cores are rare.

Much of the chromite in upper greenschist facies rocks shows somewhat transitional characteristics between types 1 and 2. Magnetite begins to penetrate along fractures instead of merely forming coatings, and the magnetite rim develops wavy, arcuate contacts against the inner chromite core (Fig. 1e), although the original morphology of the chromite is still clearly visible.

Stichtite alteration

In lower greenschist facies serpentinites from the northern Agnew–Wiluna Greenstone Belt, and particularly at Mt Keith and Honeymoon Well, chromite commonly shows pseudomorphic alteration to stichtite, a Cr-bearing layered hydroxycarbonate mineral related to pyroaurite (Ashwal & Cairncross, 1997). Chromite is typically preserved as relic cores with pseudomorphic stichtite masses preserving original lobate and poikilitic chromite mor-

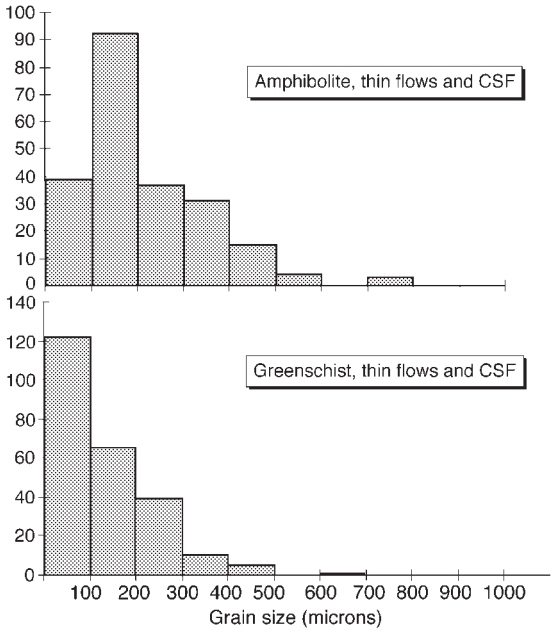

Fig. 3. Frequency distribution of apparent grain diameter (minimum dimension) of chromite (and composite type 2 chromite–magnetite grains) as a function of metamorphic grade, for samples from thin flows and channelized sheet flows (CSF) only.

phologies. Microprobe profiles of these cores show no systematic zoning related to stichtite–chromite boundaries, and chromite from this environment shows identical compositions to those from adjacent stichtite-poor rocks. It appears that the process is one of low-temperature replacement with no recognizable effect on the compositions of the relic chromite cores.

Grain size of chromite

A feature of the modification of chromite during metamorphism is a change in grain size. This can be assessed by comparing chromite grain sizes from different metamorphic grades, taking a similar range of rock types to eliminate extraneous variables. Figure 3 shows such a comparison between amphibolite and greenschist chromite, restricted to rocks from channelized sheet flows and thin differentiated flows (Barnes, 1998). This excludes dunitic rocks in which chromite is commonly lobate and very coarse; very few chromite-bearing samples of these rocks are available from amphibolite facies terrains. Data are apparent minimum grain diameters of a total of 395 grains measured in polished sections of 54 samples, and include magnetite rims.

It is apparent that amphibolite facies metamorphism introduces a significant increase in grain size. Seventy-seven percent of greenschist facies grains are <200 mm in size in minimum apparent diameter, and 50% <100 mm, compared with 59% and 18%, respectively, for amphibolite facies chromite. Medians are 100 mm and 200 mm, respectively. Two possible mechanisms may be advanced for this change: annealing and recrystallization of clusters of small grains into single large ones, and overgrowth of magnetite onto pre-existing chromite without (or in excess of) concurrent replacement of the chromite core.

CHEMICAL VARIATION IN CHROMITE WITH METAMORPHIC GRADE

For purposes of the following discussion, data are subdivided according to metamorphic grade, i.e. greenschist vs amphibolite, and within the greenschist grouping by style of magnetite alteration. 'Primary' points correspond to type 1 chromite, or cores of transitional chromite grains as far as possible from magnetite veins. A further restriction on this category is that data points fall close to an observed linear anticorrelation line between MnO and $Mg/(Mg + Fe^{2+})$, shown in fig. 8 of Barnes (1998).

Primary chromite grains from dunitic bodies tend to differ from those from thinner, spinifex-bearing komatiite flow units (Barnes, 1988), and the former are overrepresented in the greenschist data set. For this reason, data are shown only for channelized sheet flows and thin differentiated flows [see Barnes (1988) for a definition of these categories] to maximize the validity of the comparison.

Host rock mineralogy

In almost all cases, the grains analysed are from Mg-rich olivine cumulate protoliths. At greenschist facies, these are typically converted to lizardite serpentinites, antigorite–carbonate rocks or talc–carbonate $\pm$ quartz assemblages, the carbonate being a mixture of magnesite and ferroan dolomite. At lower amphibolite facies, assemblages range from olivine–tremolite (with neoblastic metamorphic olivine) and olivine–antigorite to talc–carbonate $\pm$ tremolite rocks, the presence of carbonate being related to the presence of small proportions of CO_2 in the metamorphic fluid (Johannes, 1969; Will *et al.*, 1990; Barnes & Hill, 2000). At mid-amphibolite facies the stability limit of talc + magnesite is exceeded (Will *et al.*, 1990) and stable assemblages are olivine–tremolite with talc, anthophyllite or enstatite depending on fluid composition (Gole *et al.*, 1987). Chlorite is stable across the entire range of greenschist and amphibolite facies conditions, and is stable in all these assemblages. Chlorite abundance is proportional to the Al content of the

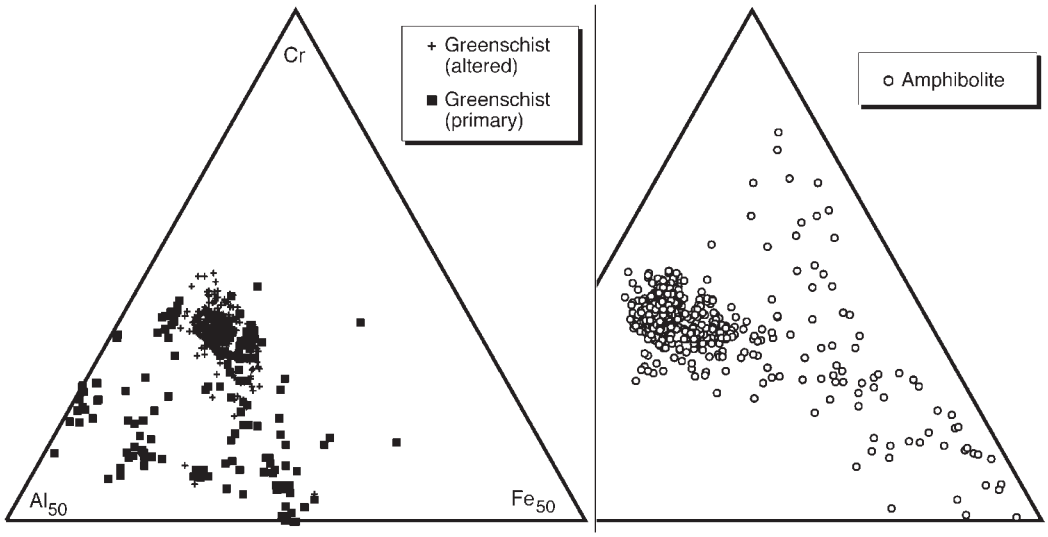

Fig. 4. Triangular cation plot for spinel compositions (type 1 grains and chromite cores of type 2 grains), showing distribution of chromite core compositions by metamorphic grade (amphibolite vs greenschist) and by nature of magnetite replacement ('altered' vs 'primary'). Data for channelized sheet flows and thin differentiated flows only.

protolith, which in turn is determined by the original trapped intercumulus liquid content.

Chromite compositions

The families of plots in Figs 4 and 5 are compilations of all currently available data on chromite in komatiites from the Eastern Goldfields, with some additional data from a variety of sources (see Appendix A). The most striking feature of all the plots in Fig. 5 is the dominant control on $Mg/(Mg + Fe^{2+})$ by metamorphic grade. Whereas greenschist chromite spans the complete range from very Mg rich to very Fe rich, amphibolite facies chromite is restricted to values of $Mg/(Mg + Fe^{2+})$ less than $\sim$0·35, and has a slight tendency towards being richer in Cr relative to Al. This is particularly true for a relatively small subset of data from high metamorphic grade (mid-amphibolite) terrains at Perseverance at Widgiemooltha. There is an extensive area of overlap on the triangular plot (Fig. 4) between amphibolite and greenschist chromite. Fe^{3+}- and Cr-poor chromite, which makes up a small but conspicuous proportion of the greenschist data set, is absent from amphibolite facies terrains.

The greatest concentration of greenschist data defines a linear array of compositions with $Mg/(Mg + Fe^{2+})$ between 0·4 and 0·7, roughly constant $Cr/(Cr + Al)$, and roughly constant and low $Fe^{3+}/(Cr + Al + Fe^{3+})$. Cobalt, Zn and Mn have weak linear negative correlations with $Mg/(Mg + Fe^{2+})$.

NiO in greenschist facies chromite (Fig. 6) tends to correlate positively with Fe^{3+} content, as would be expected on the basis of the enhanced stability of Ni in the inverse spinel structure (Barnes, 1998). TiO_2 shows a similar effect (Fig. 6). Both Ti and Ni are significantly depleted in amphibolite relative to greenschist facies chromite, although Ti shows a wide range in both amphibolite and greenschist data sets. High Ti is attributable to postcumulus igneous effects (Barnes, 1998) and appears to survive metamorphism in some cases.

Under amphibolite conditions, all $Mg/(Mg + Fe^{2+})$ values are substantially lower. $Al/(Cr + Al + Fe^{3+})$ and $Fe^{3+}/(Cr + Al + Fe^{3+})$ overlap with the greenschist data (Fig. 3), but Co, Mn and Zn all range up to very much higher values. ZnO contents in particular commonly go up to 4%, with individual outlying analyses as high as 11%. These very high Zn contents are dominantly from Kambalda and Widgiemooltha samples, and formed the basis for the assertion by Groves *et al.* (1977) that Zn-enriched spinels are diagnostic of mineralized environments. It is clear from these data that metamorphic effects play a major role.

Origin of variations in $Mg/(Mg + Fe^{2+})$

It is clear that the main difference between greenschist and amphibolite facies chromite is that the latter has significantly lower $Mg/(Mg + Fe^{2+})$. This is the consequence of the exchange of Mg and Fe^{2+} between chromite and coexisting silicates, particularly olivine, through the reaction

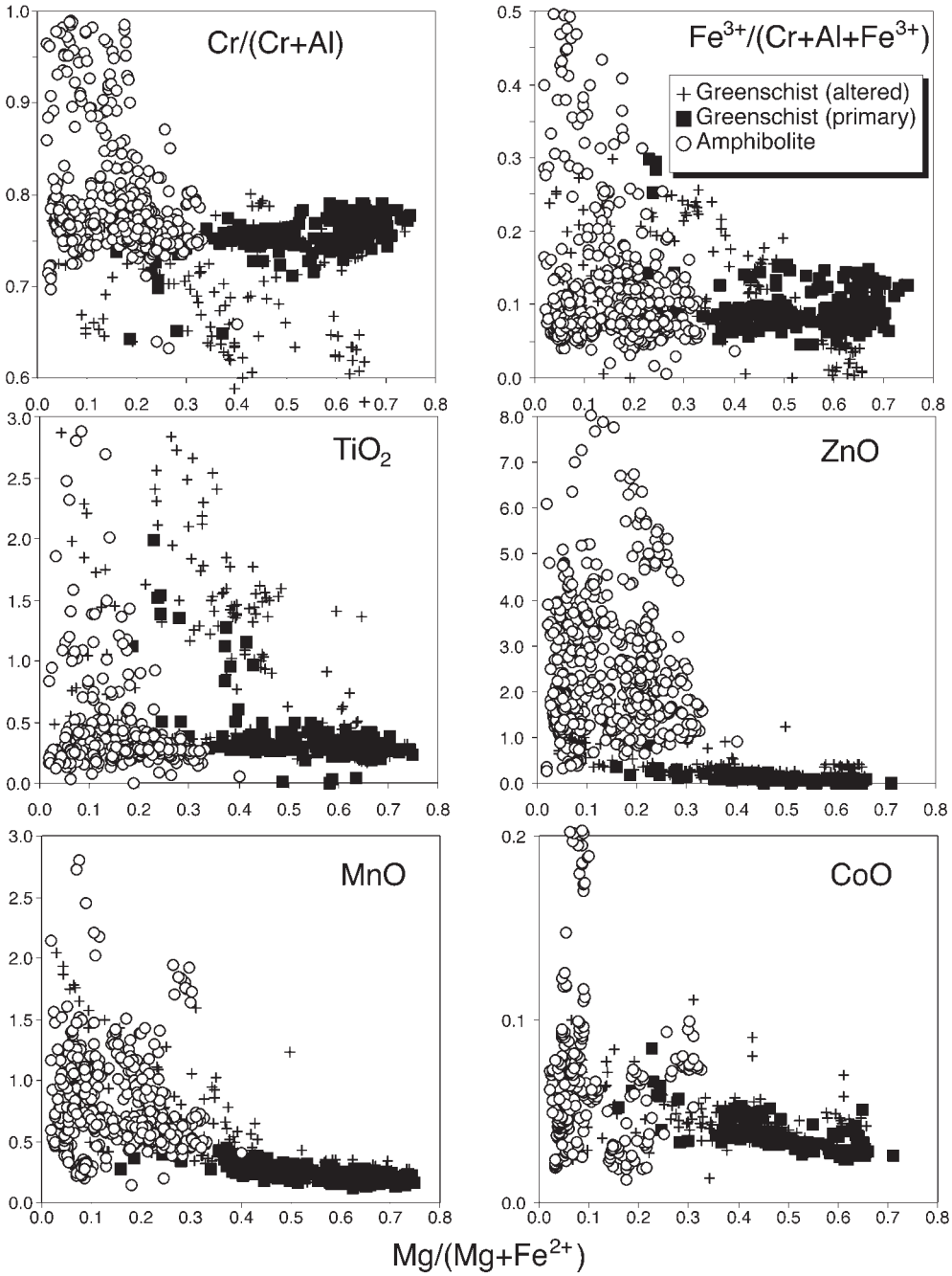

Fig. 5. Compositions of chromite cores, plotted against $Mg/(Mg + Fe^{2+})$, for chromite cores from amphibolite and greenschist facies terrains. Greenschist subdivided into 'primary' and 'altered' according to nature of magnetite replacement.

$$Mg_{spinel} + Fe^{2+}{}_{olivine} = Mg_{olivine} + Fe^{2+}{}_{spinel}.$$

The equilibrium constant for this reaction has long been known to be strongly dependent on temperature, changing in such a way that, in a given coexisting olivine–spinel pair, the olivine becomes more Mg rich and the spinel more Fe rich with falling temperature (Irvine, 1965; Jackson, 1966; Roeder *et al.*, 1979). This is the basis of the spinel–olivine geothermometer, whose calibration has most recently been updated in a comprehensive study of spinel thermochemistry by Sack & Ghiorso (1991).

Contours on spinel compositions in equilibrium with the typical range of komatiitic olivines (Fo_{94} to Fo_{88}) are shown in Fig. 7. It is clear that the temperature de-

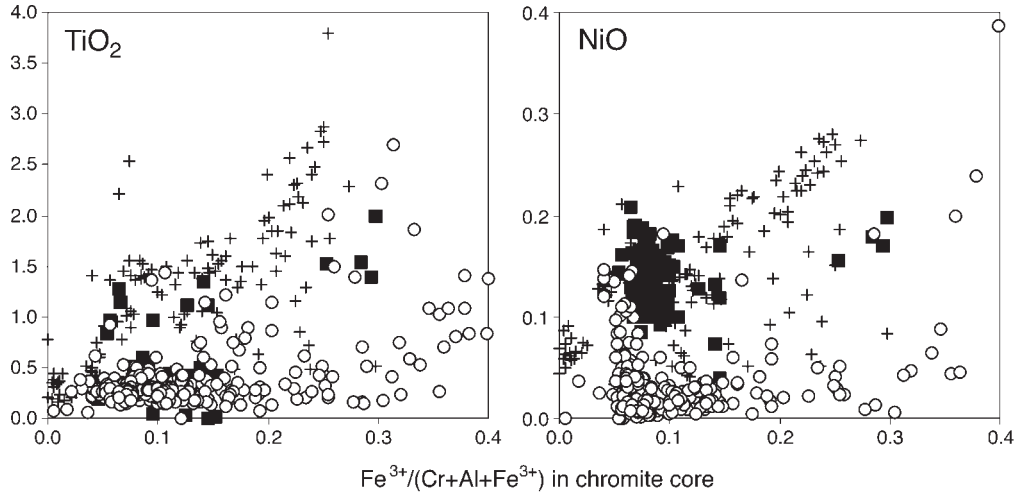

Fig. 6. NiO and TiO_2 vs $Fe^{3+}/(Cr + Al + Fe^{3+})$ in chromite cores, as a function of metamorphic grade and alteration; same data sets as for Figs 4 and 5.

pendence is very strong, and fully accounts for the metamorphic grade effect. Amphibolite facies chromite corresponds to equilibration with typical komatiitic olivine (either relic igneous or neoblastic metamorphic olivine) at temperatures around 500°C (precise temperatures cannot be read from this diagram without knowledge of individual sample details). Primary greenschist facies chromite compositions, on the other hand, imply higher equilibration temperatures, in the range 1400°C to 750°C. This apparent paradox can be explained if the 'primary greenschist' compositions are relics of the original igneous cooling stage, and have not been substantially reset during metamorphism or alteration. The observed range of temperatures extends well below the expected liquidus temperatures of komatiites, indicating varying degrees of postcumulus re-equilibration between olivine and chromite during cooling from magmatic conditions.

A complicating factor is that a significant proportion of the 'amphibolite' data come from talc–carbonate rocks at Kambalda. As discussed further below, this does not appear to produce any significantly different compositional effects, implying that exchange of Mg and Fe^{2+} between spinel, talc and ferroan magnesite operates with similar effective K_d values to those appropriate for olivine.

A significant proportion of the 'altered' greenschist data set has lower $Mg/(Mg + Fe^{2+})$ and overlaps with the amphibolite data set. This probably reflects partial re-equilibration with silicates under upper greenschist conditions.

An interesting implication of these observations is that chromite cores at amphibolite facies apparently continue to equilibrate with surrounding silicate (or carbonate) minerals despite the presence of thick magnetite rims.

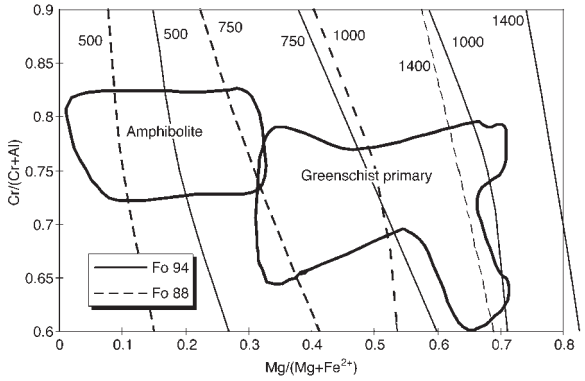

Fig. 7. Chromite compositions in equilibrium with Fo_{94} and Fo_{88} olivine at various temperatures, compared with 80th percentile fields for chromite from primary greenschist facies and amphibolite facies. Calculations use K_d values from Sack & Ghiorso (1991), average $Fe^{3+}/(Cr + Al + Fe^{3+})$ value of 0·05.

These components appear to diffuse through the magnetite, such that cores continue to communicate with the outside world.

CHEMICAL VARIATION DURING LOW-TEMPERATURE SERPENTINIZATION AND TALC–CARBONATE ALTERATION

A suite of samples from a single drill hole through the Black Swan Complex near Kalgoorlie (Fig. 1) was studied to evaluate the effects of talc–carbonate alteration. The drill hole intersects 300 m true thickness of chemically

homogeneous komatiitic olivine mesocumulates, comprising a spectrum of alteration types including partial and complete serpentinization and complete talc–carbonate alteration. Chromite was analysed from samples representing the following alteration assemblages:

- Lizardite–olivine–chlorite; incipient alteration of olivine to pseudomorphic lizardite, with >50% of the olivine remaining as fresh 'islands' in mesh-textured serpentine. Chromite is of type 1, showing very thin irregular overgrowths of magnetite.
- Antigorite–carbonate–olivine–chlorite; antigorite as parallel fibres developed as pseudomorphic replacement of olivine, with abundant relic fresh olivine, interstitial patches of fine-grained magnesite and dolomite, and typical type 1 chromite.
- Antigorite–carbonate–chlorite; complete replacement of olivine by hourglass-textured antigorite pseudomorphs with interstitial carbonate patches. Chromite shows incipient magnetite replacement along cracks, and is transitional between types 1 and 2.
- Talc–carbonate–(quartz)–chlorite–haematite; coarse porphyroblastic and poikiloblastic carbonate in a fine-grained matrix of felted talc. In some of the larger poikiloblastic carbonates the ghost of an earlier lizardite mesh texture is visible, indicating that these rocks went through an earlier phase of serpentinization. Chromites are dominantly of type 2, with extensive rims of magnetite showing well-developed external crystal faces. In some cases the chromite cores retain original lobate morphologies (Fig. 9), indicating that the magnetite is forming dominantly as an overgrowth and to a lesser extent by replacement, favouring this as the likely mechanism for the increase in spinel grain size during metamorphism. Haematite is a widespread phase in the Black Swan talc–carbonates, occurring as widely dispersed blades and laths, which in some cases are nucleated on type 2 chromite–magnetite grains.

Quartz is a common minor constituent in the talc–carbonate rocks of Black Swan, indicating that metamorphism took place at low temperatures, probably around 300°C, with fluid compositions buffered along the magnesite + quartz = talc reaction curve (Barnes & Hill, 2000). The talc–carbonates apparently formed during late-stage CO_2 metasomatism of previously serpentinized rocks, under oxidizing conditions at relatively low fluid:rock ratios.

Compositions of chromite cores from the different alteration facies are plotted in Fig. 8. Alteration style is the only source of variation between these samples.

The main consequence of the alteration process is exchange of Mg and Fe^{2+}. Chromite in rocks retaining fresh olivine retains primary igneous $Mg/(Mg + Fe^{2+})$ ratios, but both talc–carbonate and antigorite–carbonate rocks without fresh olivine are significantly depleted in Mg. In rare cases, coarse chromite from talc–carbonate rocks is zoned with respect to $Mg/(Mg + Fe^{2+})$ (Fig. 9), the ratio ranging from 0·5 to 0·66.

Mg depletion is accompanied by essentially no change in the $Cr/(Cr + Al)$ ratio, a slight but significant decrease in Fe^{3+}, a slight decrease in Ni and a large increase in Co and Zn. Mn shows a wide and unsystematic variation in the serpentinites, but is relatively depleted in the talc–carbonate rocks.

These changes can be attributed to a combination of factors: the release of divalent ions from olivine during serpentinization, and competition for elements between carbonate, chromite and newly formed magnetite growing as rims on chromite. Magnetite development corresponds to the major change in oxidation state going from highly reduced conditions at the serpentinization front (Frost, 1985) to the highly oxidized conditions recorded by the presence of haematite in the talc–carbonate rocks. Nickel is partitioned preferentially into magnetite, whereas Co, Mn and Zn released from olivine during serpentinization are preferentially taken up by chromite. Mg and Mn are incorporated into carbonate minerals through Fe–Mn and Fe–Mg exchange reactions, leaving chromite strongly depleted in these elements during subsequent replacement of serpentine by talc–carbonate assemblages.

ZONING AND WITHIN-GRAIN ELEMENT DISTRIBUTIONS

Detailed understanding of the data presented so far depends on understanding how elements are distributed within grains, particularly in zoned type 2 composite grains and in altered greenschist facies grains. This is addressed here through two-dimensional X-ray intensity maps, obtained on the electron microprobe, showing distributions of selected elements.

Figures 9 and 10 show the transition from type 1 chromite with incipient replacement along rims and magnetite veins to true type 2 chromite undergoing progressive replacement by magnetite. Both samples are from the eastern Ultramafic Complex at Mt Keith and are at the same regional metamorphic grade. The sample illustrated in Fig. 10 has undergone extensive CO_2 infiltration resulting in development of an antigorite–carbonate alteration assemblage.

Relic igneous zoning is evident in the first grain (Fig. 10) in the form of zoning with respect to Al and particularly Ti (Fig. 11). This concentric zoning pattern is completely overprinted by a pattern of anastomosing magnetite-rich veins, showing up as high Fe. Mn and Zn show maximum concentrations immediately adjacent to the veins, as can be seen most clearly in the large veins on the right-hand edge and top left of the field of view. It is clear that both

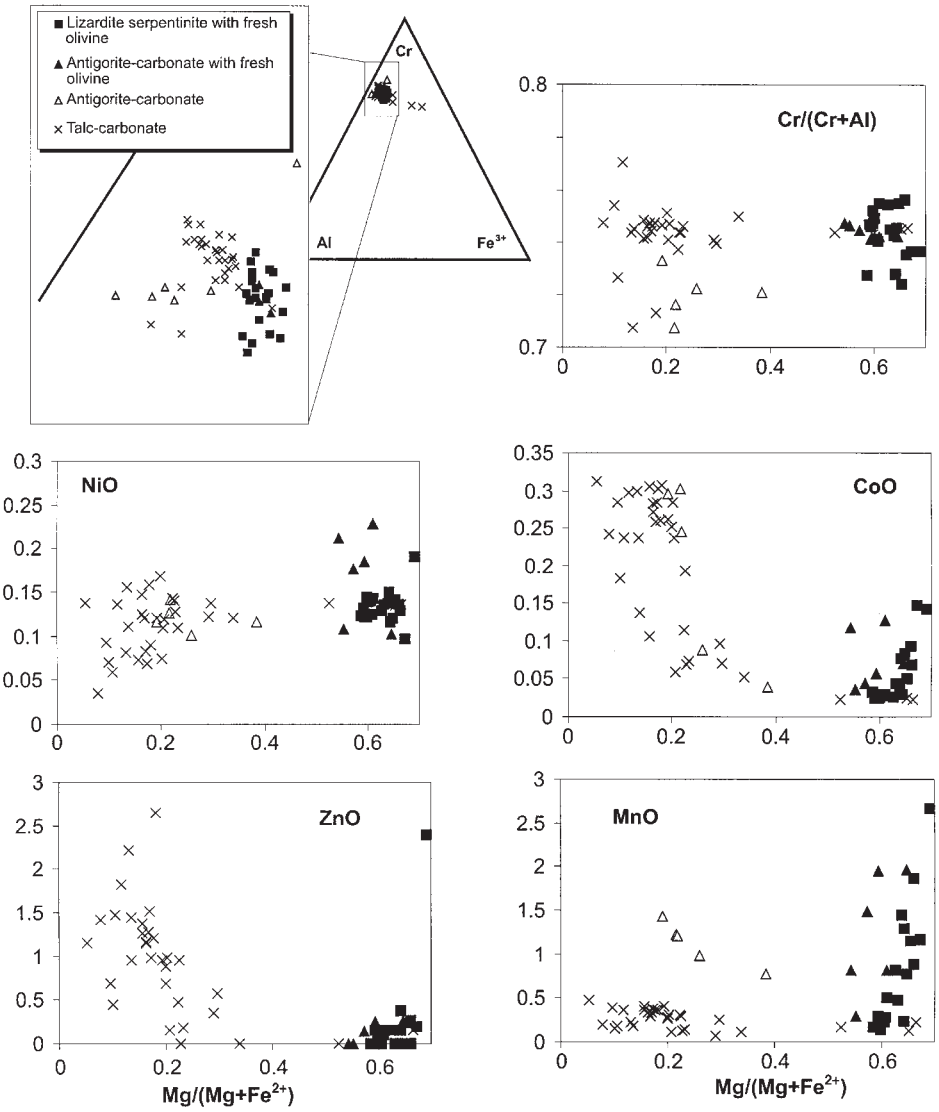

Fig. 8. Compositions of chromite cores in different alteration facies from a suite of chemically identical olivine mesocumulate rocks, Black Swan Complex.

Zn and Mn were introduced during the alteration process, being concentrated into the chromite at the vein walls from the infiltrating metamorphic fluid.

In the case of more advanced magnetite replacement (Fig. 11), Zn shows a very pronounced concentric zonation, from typically primary values around 0·2% in the core to nearly 3% immediately adjacent to the magnetite rim (Fig. 12). A complete spectrum of distributions is observed between this and the previous pattern, indicating that this distribution is not primary, but rather the result of the introduction of Zn during fluid interaction. In this case, this pattern is not shared by Mn, which is probably due to the presence of abundant carbonate, a favourable sink for Mn, in the host mineral assemblage.

Indication of the timing of Zn and Mn introduction is given by the presence of similar patterns to that in Fig. 10 in a lobate chromite from low-grade, weakly serpentinized olivine adcumulate in the Mt Clifford–Marshall Pool area (Fig. 13). This differs from the Mt Keith examples in that olivine is mostly fresh in this rock. It is clear from these maps that Zn, Mn and Fe are all introduced into the chromite during alteration, which must have accompanied the early stages of serpentinization of olivine. It is possible that the introduced Zn and Mn were derived from the immediately adjacent olivine.

With increasing metamorphic grade, the heterogeneous distributions of minor elements noted so far are partially

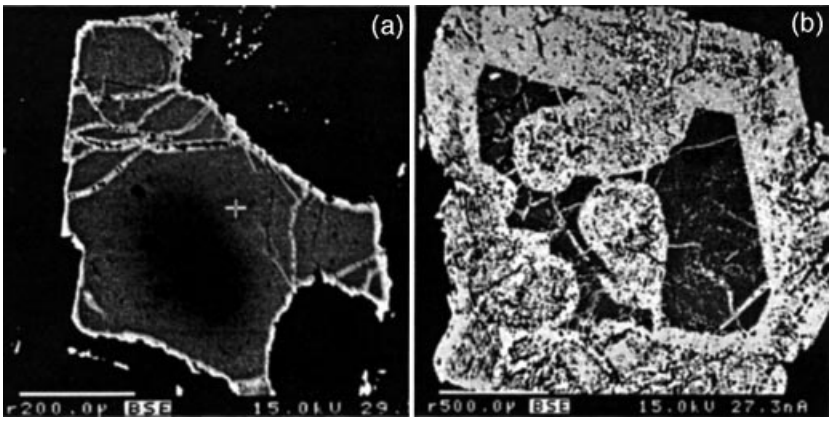

Fig. 9. Back-scattered electron micrographs of chromite from low-temperature alteration assemblages at Black Swan. (a) Zoning in Mg–Fe (Mg-rich core, Mg-poor margin) in lobate chromite from talc–carbonate, sample BSD112-211.0. (b) Type 2 chromite, showing retention of original lobate morphology by chromite core, talc–carbonate sample BSD112-420.9.

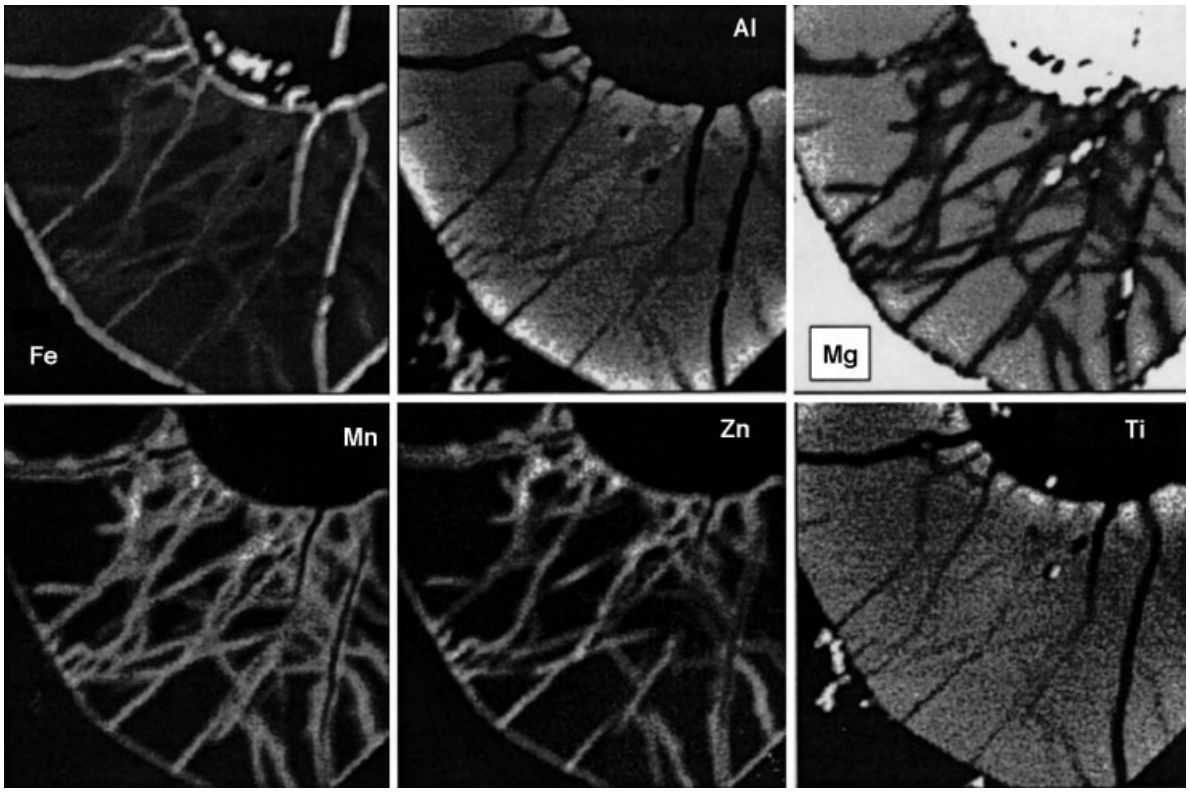

Fig. 10. X-ray maps of major and minor element distribution in a transitional type 1 chromite showing incipient alteration along rims and cracks. Sample of lizardite serpentinite after olivine orthocumulate, B zone of thin flow in Mt Keith Lower Flow sequence. Lighter grey indicates higher concentrations. Range of Mn in chromite from 0·2 to 3·0%, Zn from 0·1 to 1·5%. Field of view 0·5 mm.

homogenized by diffusion within the chromite core, whereas strong zonation appears within the magnetite rims. This progression is illustrated in Figs 14 and 15. A type 2 chromite from a talc–carbonate altered olivine mesocumulate from Kambalda, representing lower amphibolite facies (Fig. 14), is contrasted with advanced type 2 replacement of a chromite from a serpentinized olivine–tremolite–chlorite rock from mid-amphibolite facies conditions at Windarra (Fig. 15).

Zinc in the chromite core is almost completely homogenized in both cases, but clearly elevated well above the range found in cores at lower metamorphic grades.

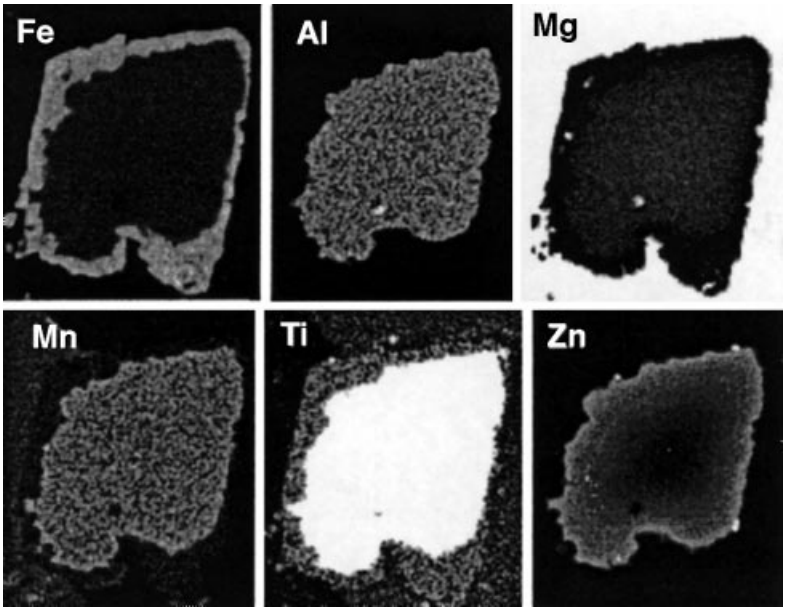

Fig. 11. X-ray maps showing major and minor element distribution in a type 2 chromite in antigorite–carbonate rock, Mt Keith Ultramafic Complex Zone D. Lighter grey indicates higher values, range in ZnO 0·3–3·0%. Field of view 250 mm.

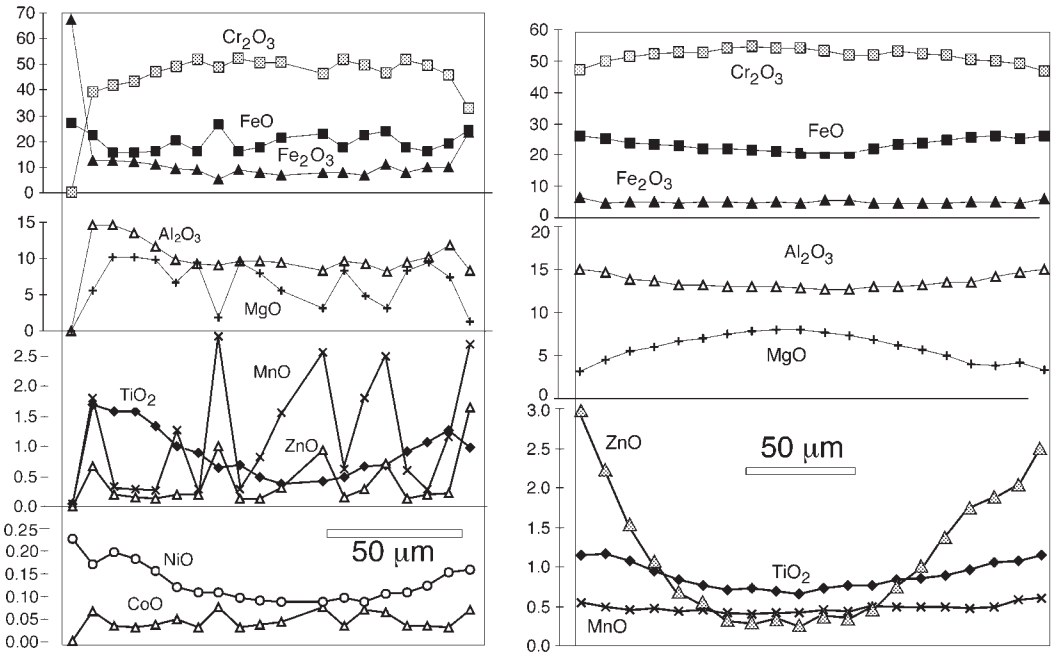

Fig. 12. Quantitative microprobe profiles of major and minor elements across chromite grains shown in Fig. 10 (left) and Fig. 11.

This points to a continuing process whereby Zn is continuously introduced by fluid interaction during progressive metamorphism, and progressively homogenized within the chromite core, a process enhanced by more rapid diffusion at higher temperatures. In the Windarra case, under these conditions Zn also begins to diffuse, along with Cr and Ti, into the magnetite rim, giving rise to a typical parabolic concentration profile through the magnetite away from the chromite core. Manganese behaves in a very similar way to Zn, as seems generally to be the case in the absence of competing carbonate phases.

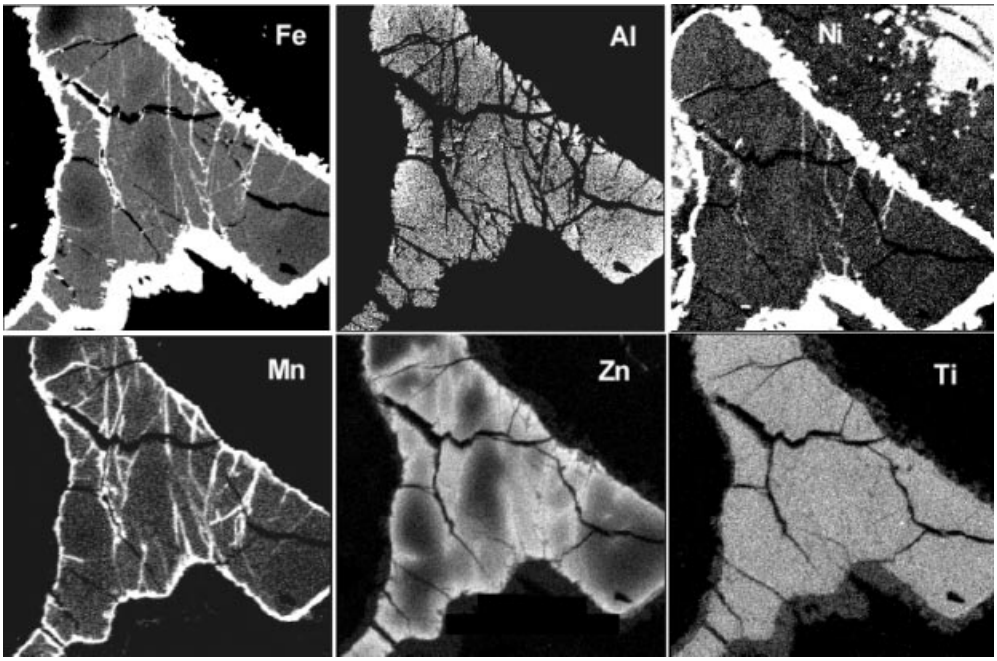

Fig. 13. X-ray maps of major and minor element distribution in a type 1 chromite in partially serpentinized dunite, Mt Clifford Ultramafic Complex. Light grey indicates higher values. White in Fe map indicates magnetite rim. ZnO ranges from 0·1 to 1·0%. Field of view 0·5 mm.

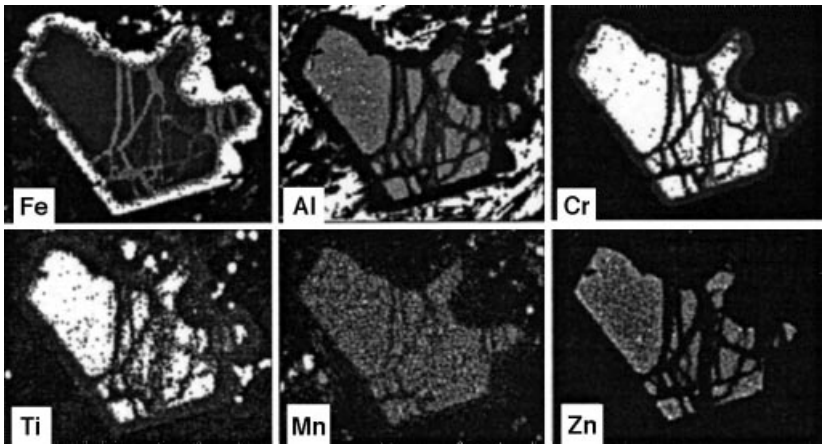

Fig. 14. X-ray intensity maps of veined type 2 chromite in talc–carbonate rock. Kambalda, Hunt Shoot traverse, sample KD275-676.5, field of view 0·5 mm. Range in ZnO in chromite core 1·4–1·75%.

Titanium in the Windarra sample shows a sharp peak (more clearly visible on the X-ray map than on the quantitative profile) corresponding to the innermost boundary of the magnetite rim. This is a consequence of a relatively slow rate of diffusion for Ti in magnetite: Ti partitions from the chromite into the magnetite rim, but 'piles up' at the grain boundary as diffusion is too slow to even out the profile. Ti is relatively homogeneous within the chromite core, implying that the rate of diffusion is higher in the chromite than in the magnetite.

Cobalt follows Zn and Mn, being mainly concentrated in the chromite core but showing a diffusion profile out into the magnetite (Fig. 16). Nickel is almost entirely concentrated in the magnetite, showing a slight increase towards the outside of the grain. This is probably an equilibrium profile, reflecting high diffusion rates, and a strong tendency for Ni to substitute on the octahedral sites in the inverse spinel structure of magnetite.

Origin of Zn enrichment in komatiitic chromite

Groves *et al.* (1977) postulated a genetic association between Zn-enriched chromite and komatiite-hosted mag-

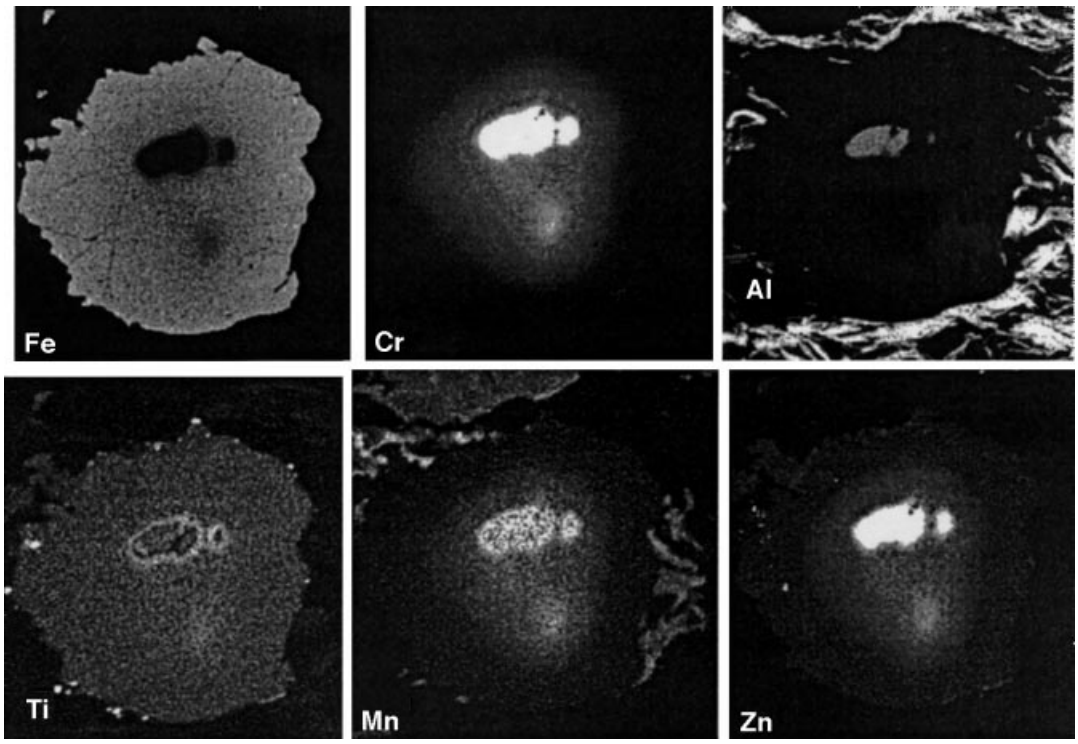

Fig. 15. X-ray intensity map of type 2 chromite with advanced magnetite replacement, Windarra. Field of view 0·5 mm. Strong zoning of Cr and Fe in magnetite, and ring of high Ti corresponding to innermost edge of magnetite rim, should be noted.

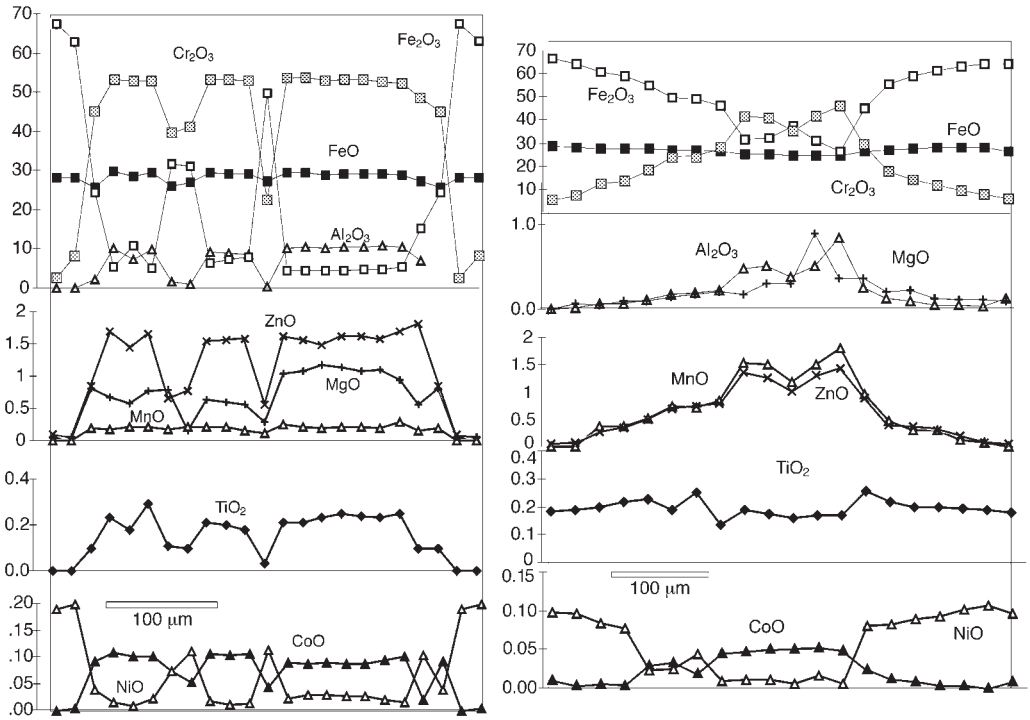

Fig. 16. Quantitative microprobe profiles across Kambalda zoned chromite (left) shown in Fig. 14, and Windarra zoned chromite (right) shown in Fig. 15.

matic Ni sulphide deposits, largely on the basis of the abundance of Zn-enriched chromite at Kambalda. Parker (1984) showed a close association at Widgiemooltha between highly Zn-enriched spinel, mineralization and the presence of Zn-enriched interflow sulphides.

The observations reported here indicate that the process of Zn enrichment is entirely secondary, in line with the conclusions of Wylie *et al.* (1987). Greenschist facies chromite is almost entirely low in Zn, particularly those primary grains that have $Mg/(Mg + Fe^{2+})$ values >0·3. Significantly, high Zn contents in excess of 1% are restricted to chromite that has undergone metamorphic exchange. Furthermore, Zn contents in excess of 2% are restricted to the cores of type 2 grains in amphibolite facies rocks, and are never observed in primary greenschist facies chromite, whether in mineralized sequences or not. These observations argue strongly that Zn enrichment is a metamorphic effect, related to introduction of Zn during hydrothermal alteration and subsequent recrystallization. The strong similarity in the distribution of Mn and Co to that of Zn (Fig. 5) implies that these elements are also introduced during metamorphism and alteration. This conclusion is very strongly supported by detailed observations on the distribution of these elements within altered chromite.

The highly Zn-enriched spinel at Widgiemooltha may still be related to the proximity of Zn-enriched sulphidic sediments. These may be instrumental both in providing a source for secondary Zn enrichment and a source for primary magmatic sulphur (Lesher *et al.*, 1984). However, moderate enrichment in Zn in chromite from partially fresh, unmineralized rocks at Mt Clifford with no adjacent Zn-rich sediments argue that much of the additional Zn in altered chromite is released from the originally adjacent olivine.

Manganese in chromite in greenschist facies serpentinites

In detail, the behaviour of Mn associated with secondary magnetite alteration is complex and curious. Figure 17 shows data from a suite of samples from the low greenschist facies, serpentinized Mt Keith complex, including grains such as the one illustrated in Fig. 10.

Two linear trends are visible in Fig. 17. The lower trend shows a slight linear increase in MnO with decreasing $Mg/(Mg + Fe^{2+})$, typical of 'primary' trends seen in lower greenschist facies rocks (Barnes, 1998). This trend incorporates samples from the three alteration facies recognized in the complex: typical lizardite serpentinites, antigorite–carbonate assemblages, and lizardite serpentinites in which the chromite shows extensive marginal pseudomorphic alteration to stichtite. Diverging from this trend at $Mg/(Mg + Fe^{2+})$ around 0·45 is a second, steeper linear trend, defined by stichtite-free lizardite serpentinite samples, including the grain illustrated in Fig. 10. The Mn-enriched points along this trend are all clearly related to marginal enrichment in Zn and Mn adjacent to thin magnetite veinlets as shown in Fig. 10, and these points are all irregularly enriched in Zn and Co.

The origin of this feature remains a mystery. The steep linear trend may record the presence of a submicroscopic exsolved or intergrown Mn-enriched phase developed next to the magnetite veinlets, with the probe beam analysing a mixture of the two phases. However, the nature of this hypothetical phase is unknown. A similar phenomenon has been noted in other chromite from lizardite serpentinites, including some samples from the Zangbutai ultramafic body in China (Barnes & Tang, 1999), indicating that it is a general phenomenon.

VARIATION IN AMPHIBOLITE FACIES SPINELS

Some significant variations are apparent between chromite core compositions at different amphibolite facies localities, as shown in Figs 18 and 19.

Kambalda chromite is most tightly clustered and generally shows the lowest values of $Mg/(Mg + Fe^{2+})$ compared with other localities. This may be due to the widespread talc–carbonate alteration and the fact that Kambalda chromite equilibrated with abundant metamorphic carbonate minerals, capable of carrying Fe^{2+}. The trivalent ions in the Kambalda chromite are very similarly distributed to those in greenschist facies 'primary' chromite, implying that relatively little redistribution of these elements occurred under lower amphibolite talc–carbonate conditions.

Anomalously low Al and highly variable Fe^{3+} contents are observed in several localities, most significantly Perseverance and Widgiemooltha, where metamorphic grades are somewhat higher and metamorphic olivine is widespread (Fisher, 1979; McQueen, 1979, 1981; Gole *et al.* 1987). At Perseverance in particular, type 2 chromite underwent particularly advanced replacement by magnetite, and these grains are very commonly mantled by chlorite. The observed compositional effect is likely to be the result of metamorphic exchange of Al and Fe^{3+} between chromite and chlorite, with Al favouring the chlorite structure. This effect is restricted to a relatively small proportion of grains at each locality, however, implying that full equilibrium has not been attained. The extent of reaction may be a function of fluid–rock ratios and the extent to which the exchange and replacement reactions are driven by fluid influx.

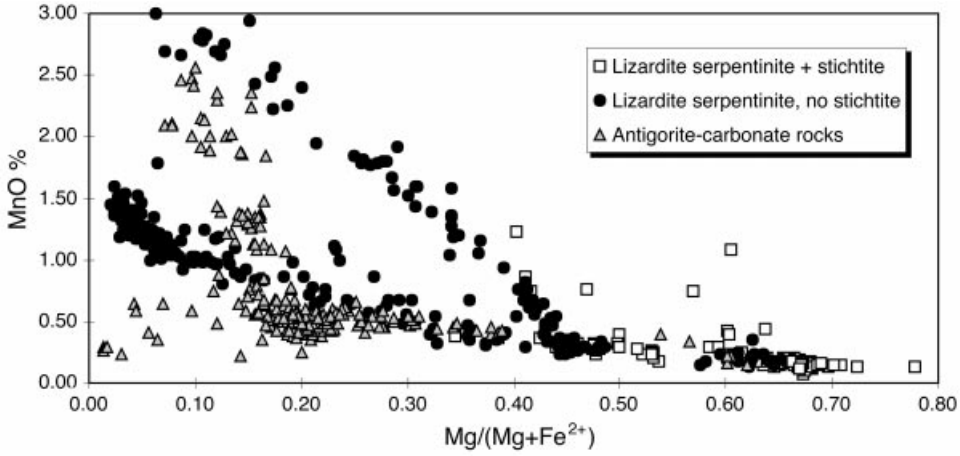

Fig. 17. MnO contents of chromite cores, individual points from traverses across grains, from the Mt Keith Eastern Ultramafic Complex. Samples subdivided by alteration facies.

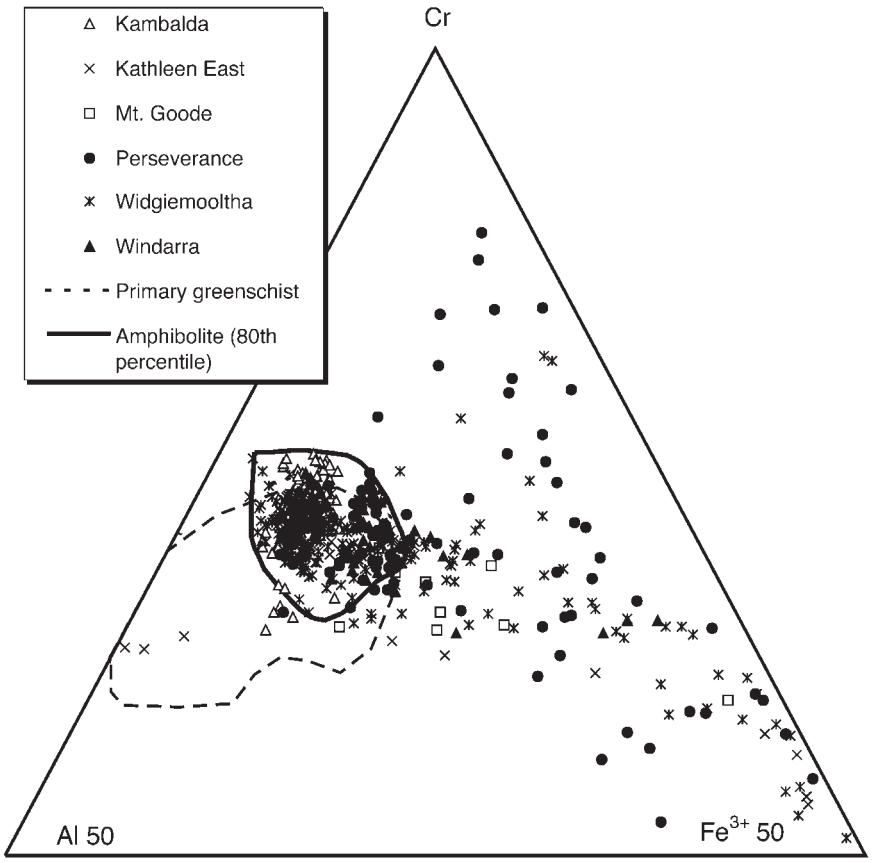

Fig. 18. Trivalent ion plot (from 50 to 100% Cr) for chromite cores from various amphibolite facies localities, showing 80th percentile data density contour, compared with field for 'primary' type 1 chromite cores from greenschist facies localities. Perseverance and Windarra represent mid-amphibolite facies conditions, chromite coexisting with chlorite, tremolite and metamorphic olivine. Kathleen East and Mt Goode, uppermost greenschist facies, serpentinites; Kambalda, lower amphibolite facies, mainly talc–carbonate rocks; Widgiemooltha, low to mid-amphibolite, serpentinites, some metamorphic olivine.

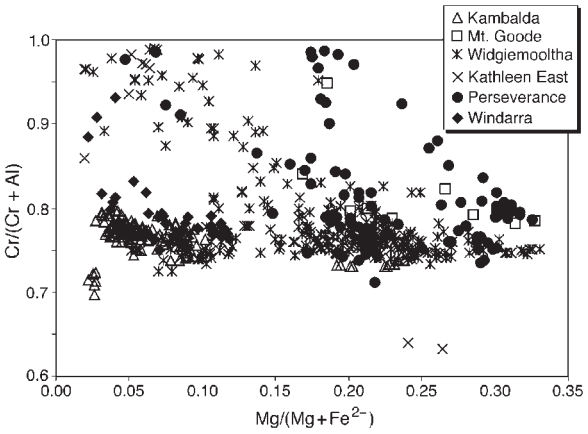

Fig. 19. Chromite compositions (vs *mg*-number) from amphibolite facies localities, corresponding to data in Fig. 18.

Magnetite–chromite immiscibility—an indicator of peak metamorphic temperature?

A further factor influencing the development of more Fe^{3+}-enriched chromite cores is the diminishing size of the miscibility gap between chromite and magnetite with increasing temperature. Referring to the theoretical phase diagram of Sack & Ghiorso (1991), and considering chromite in equilibrium with Fo_{90} olivine, there is complete solid solution from chromite to magnetite at 600°C but a significant miscibility gap which widens rapidly below 550°C (Fig. 20). A plausible explanation for type 2 chromite is that the core and rim represent coexisting chromite and magnetite on either side of the miscibility gap.

Major changes in the shape of the spinel stability fields occur around the temperatures of lower- to mid-amphibolite facies metamorphism, within the range of compositions in equilibrium with typical komatiitic olivines. The wide range in spinel compositions at Perseverance, corresponding to metamorphism around 550°C, is consistent with the near-disappearance of the chromite–magnetite miscibility gap at this temperature. The absence of low-Fe^{3+}, relatively high-Al 'primary' chromite from amphibolite facies rocks may reflect the appearance of a large immiscibility gap between chromite and Mg–Al-rich spinel. It is unlikely that the Sack and Ghiorso miscibility gaps correspond exactly to the natural spinels, allowing for the presence of minor components and the uncertainties in the thermodynamic data, but they appear to be generally consistent with the data. Major-element compositions of chromite–magnetite pairs are therefore reasonably sensitive indicators of metamorphic grade, as illustrated in Fig. 20.

The Sack and Ghiorso stability fields are compared in Fig. 20 with data from microprobe traverses across type 2 grains from three amphibolite facies localities, Perseverance, Kambalda and Windarra, and one lower greenschist facies locality, Honeymoon Well. Traverse data were used to give as closely as possible compositions of coexisting chromite and magnetite across the core–rim boundary. In all cases, data were collected at intervals of 4–10 μm, and the point closest to the boundary was discarded to allow for possible grain boundary effects.

At Perseverance, there is a very small miscibility gap between chromite cores and magnetite rims, the rims contain large amounts of Cr, and most of the cores are markedly depleted in Al. This suggests that the Perseverance spinels equilibrated at some temperature between 550 and 600°C consistent with previous work (Gole *et al.*, 1987), and that the miscibility gap between chromite and magnetite begins to open up in this range at a fairly Cr-rich composition. At Kambalda and Windarra (neglecting a few points which may have straddled a phase boundary) the miscibility gap is much wider, and consistent with the Sack and Ghiorso model at around 500°C, again consistent with previous work (Archibald *et al.*, 1978). Furthermore, at these two localities a large proportion of the chromite cores plot within the primary magmatic field and do not appear to have re-equilibrated completely with the magnetite rims. At Honeymoon Well, in complete contrast, many of the core compositions plot outside the Sack and Ghiorso 600°C field, indicating relic magmatic compositions not affected by metamorphism. Magnetite rims are almost pure magnetite with very limited Cr solubility, implying magnetite growth well below 500°C.

On the basis of this analysis, it appears that as far as trivalent ions are concerned, chromite in lowest amphibolite facies rocks, i.e. equilibrated below ~500–550°C, retains original igneous chemistry. However, $Mg/(Mg + Fe^{2+})$ values are substantially lowered by Fe–Mg exchange with silicates and/or carbonates. Metamorphism in the 550–600°C range, as at Perseverance and Widgiemooltha, marks the limiting condition where igneous compositions are substantially modified by equilibration between chromite cores, magnetite rims, and surrounding silicates such as chlorite. Loss of Al from chromite cores to chlorite takes place through the medium of infiltrating metamorphic fluids, as suggested by Wylie *et al.* (1987).

CONCLUSIONS

The data presented above provide a picture of the chemical modification of chromite during lower greenschist alteration and subsequent amphibolite facies metamorphism, processes which are probably continuous with one another. Low-temperature serpentinization produces incipient development of slightly Fe-enriched chromite

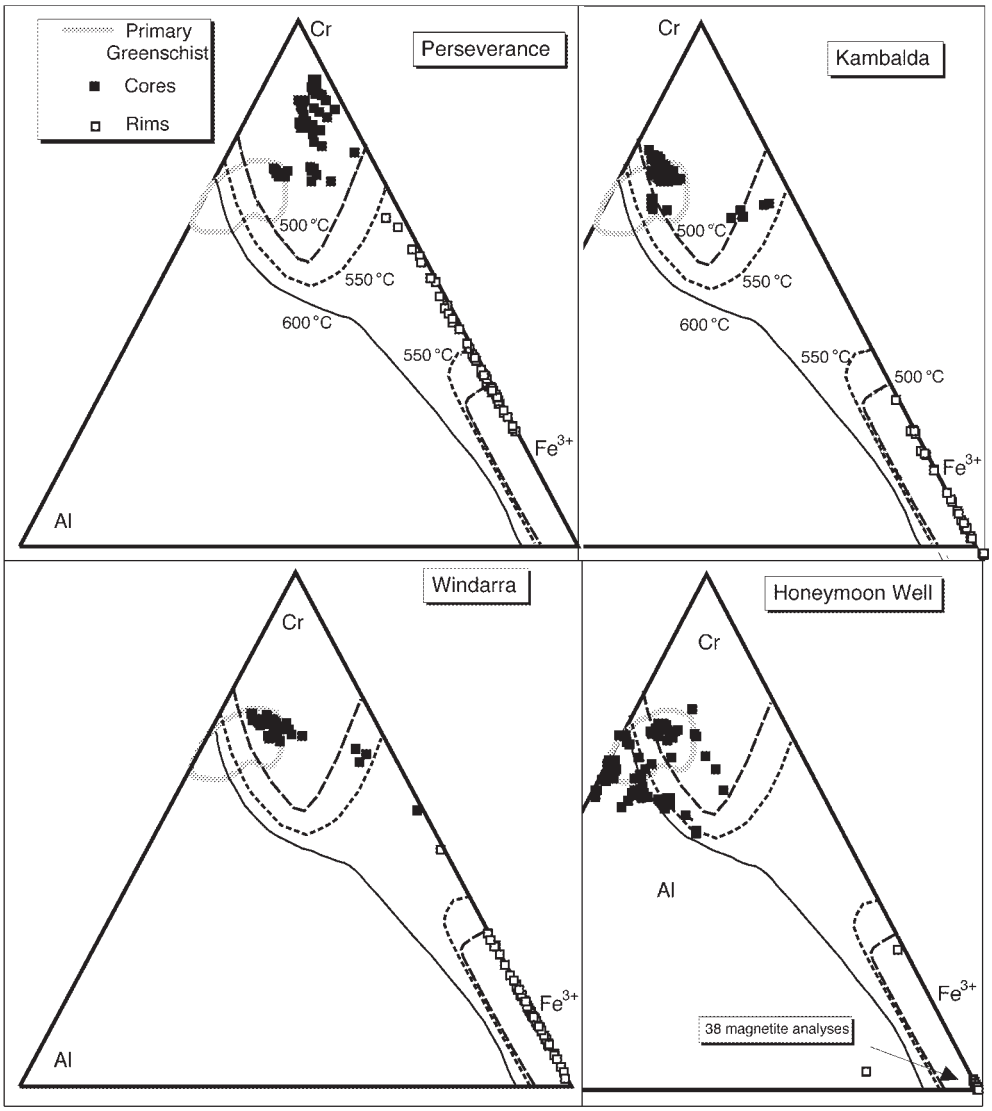

Fig. 20. Sack and Ghiorso spinel stability limits for chromite and magnetite (calculated for equilibrium with olivine of composition Fo_{90}), compared with data for spinel analyses from across-grain traverses from Kambalda, Perseverance, Windarra and Honeymoon Well (see Fig. 1 for locations).

adjacent to pure magnetite veinlets, as a result of fluid ingress along cracks and around the grain boundaries of the chromite. This material is also strongly enriched in Zn, and also in Mn unless there is substantial carbonate in the alteration assemblage. Further fluid ingress and reaction at higher temperatures results in extensive replacement of chromite by magnetite, further introduction of Zn (and possibly Mn) into the chromite, and interdiffusion of elements between chromite and magnetite. Prolonged diffusion of elements at elevated metamorphic temperatures results in homogenization of the Zn-enriched chromite core, and development of the complex multi-element zoning in Cr-bearing magnetite.

Metamorphism also involves equilibration of the chromite core with the surrounding silicate assemblage. Exchange of Fe and Mg happens readily through upper greenschist and lower amphibolite facies, whereas relative proportions of the trivalent ions remain close to magmatic values up to lower amphibolite conditions of ~500–550°C. Above this temperature more radical

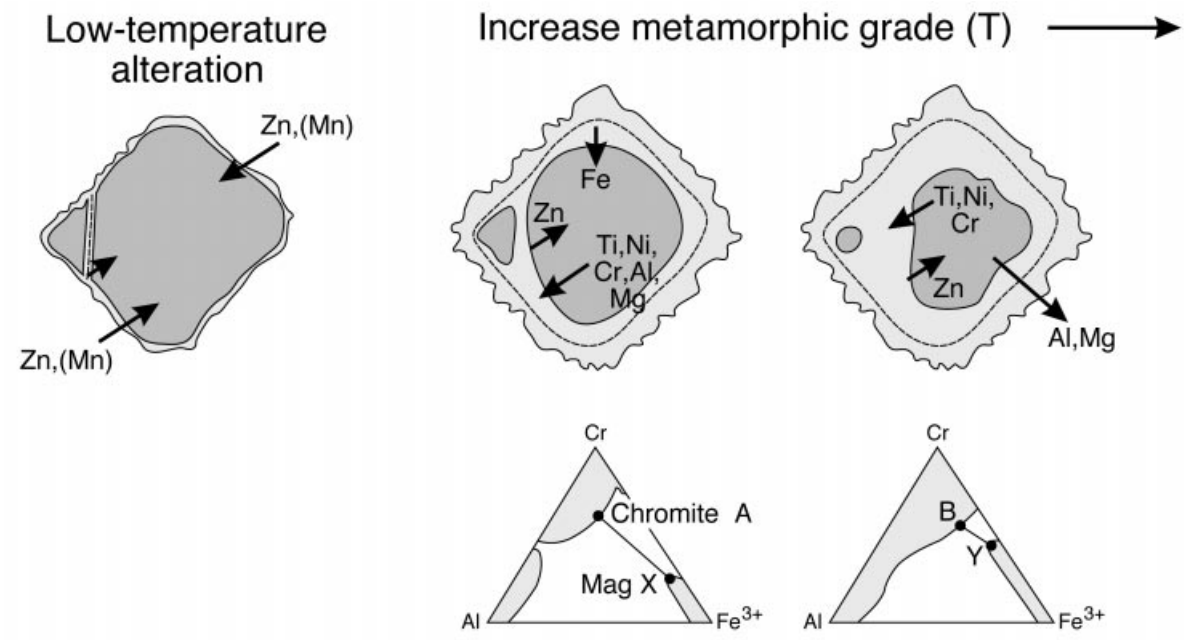

Fig. 21. Schematic illustration of chemical changes in chromite cores and magnetite rims during progressive alteration and metamorphism of chromite.

modification of chromite cores occurs as a result of small-scale equilibration with infiltrating fluids; effectively, fluids transfer Al from chromite to chlorite. Hence, as well as element redistribution within grains there is significant redistribution between grain and matrix.

These processes are summarized in Fig. 21, a schematic illustration of the processes of alteration and metamorphic reconstitution of chromite. The simplified phase diagrams show the extent of the spinel miscibility gap appropriate to that stage of the process. Low-temperature alteration and metamorphism are seen as a more or less continuous process of re-equilibration and replacement of chromite by magnetite. The extent of replacement in any given sample is largely a matter of fluid access and fluid–rock ratio; where fluid–rock interactions are fluid dominant, chromite is almost completely destroyed, and chromite undergoes extensive Al loss to surrounding chlorite. High fluid–rock ratios are the case at Perseverance (Gole *et al.*, 1987), where very little chromite survives in any host rock.

This view of chromite–magnetite relationships has chromian magnetite rims forming as an essential component of the prograde metamorphic assemblage. This study supports the conclusions of Wylie *et al.* (1987), who interpreted magnetite rims as precipitating from a fluid in local equilibrium with chromite undergoing dissolution. Effectively, magnetite is the product of fluid-driven reaction between chromite and surrounding chlorite. Continuing equilibration between chromite cores and magnetite rims records metamorphic conditions in a fairly sensitive way. Future work may show that complex zoning patterns in chromian magnetite rims are indicators of metamorphic cooling paths.

ACKNOWLEDGEMENTS

This study was carried out as part of a project funded by Western Mining Corporation Resources Ltd., whose financial support is gratefully acknowledged. Thanks are due to Bruce Robinson, Nerida Reilly and Greg Hitchen, who provided assistance with microprobe analyses, and Dr Thor Thordarson and Professor Richard Arculus, who reviewed the manuscript.

REFERENCES

Abzalov, M. Z. (1998). Chrome-spinels in gabbro–wehrlite intrusions of the Pechenga area, Kola Peninsula, Russia: emphasis on alteration features. *Lithos* **43**, 109–134.

Allen, R. L. (1990). Petrology and chemistry of a komatiite sill and Fe–Ni–Cu sulphide mineralization, Munro and Beatty Townships, Ontario. M.Sc. thesis. Queens University: Kingston, Ontario.

Archibald, N. J., Bettenay, L. F., Binns, R. A., Groves, D. I. & Gunthorpe, R. J. (1978). The evolution of Archean greenstone terrains, Eastern Goldfields Province, Western Australia. *Precambrian Research* **6**, 103–131.

Arndt, N. T., Naldrett, A. J. & Pyke, D. R. (1977). Komatiitic and iron-rich tholeiitic lavas of Munro Township, northeast Ontario. *Journal of Petrology* **18**, 319–369.

Ashwal, L. D. & Cairncross, B. (1997). Mineralogy and origin of stichtite in chromite-bearing serpentinites. *Contributions to Mineralogy and Petrology* **127**, 75–86.

Barnes, S. J. (1998). Chromite in komatiites, 1. Magmatic controls on crystallization and composition. *Journal of Petrology* **39**, 1689–1720.

Barnes, S. J. & Hill, R. E. T. (2000). Metamorphism of komatiite hosted nickel sulfide deposits. *Reviews in Economic Geology* **11** (in press).

Barnes, S. J. & Tang, Z. (1999). Chrome spinels from the Jinchuan Ni–Cu sulphide deposit, Gansu Province, People's Republic of China. *Economic Geology* **94**, 343–356.

Barnes, S. J., Lesher, C. M. & Keays, R. R. (1993). Geochemistry of mineralised and barren komatiites from the Perseverance Mine area. CSIRO Division of Exploration Geoscience Restricted Report **336R**, 41 pp.

Blais, S. & Auvray, B. (1990). Serpentinization in the Archean komatiitic rocks of the Kuhmo greenstone belt, eastern Finland. *Canadian Mineralogist* **28**, 55–66.

Bliss, N. W. & MacLean, W. H. (1975). The paragenesis of zoned chromite from central Manitoba. *Geochimica et Cosmochimica Acta* **39**, 973–990.

Burkhard, D. J. M. (1993). Accessory chrome spinels: their co-existence and alteration in serpentinites. *Geochimica et Cosmochimica Acta* **57**, 1297–1306.

Donaldson, M. J. (1981). Redistribution of ore elements during serpentinisation and talc–carbonate alteration of some Archaean dunites, Western Australia. *Economic Geology* **76**, 1698–1713.

Donaldson, M. J. (1983). Progressive alteration of barren and weakly mineralised Archaean dunites from Western Australia: a petrological, mineralogical and geochemical study of some komatiitic dunites from the Eastern Goldfields Province. Ph.D. thesis. University of Western Australia: Nedlands, Western Australia, 345 pp.

Evans, B. W. & Frost, B. R. (1975). Chrome spinel in progressive metamorphism—a preliminary analysis. *Geochimica et Cosmochimica Acta* **39**, 959–972.

Fisher, D. (1979). The petrology of the Mt. Edwards nickel sulphide deposit, Widgiemooltha, Western Australia. Ph.D. thesis, University of Toronto.

Frost, B. R. (1985). On the stability of sulfides, oxides and native metals in serpentinite. *Journal of Petrology* **26**, 31–63.

Frost, K. M. & Groves, D. I. (1989). Magmatic contacts between immiscible sulfide and komatiitic melts; implications for genesis of Kambalda sulfide ores. *Economic Geology* **84**, 1697–1704.

Gole, M. J. & Hill, R. E. T. (1990). The refinement of extrusive models for the genesis of nickel deposits: implications from case studies at Honeymoon Well and the Walter Williams Formation. Minerals and Energy Research Institute of Western Australia Report **68**, 93 pp.

Gole, M. J., Barnes, S. J. & Hill, R. E. T. (1987). The role of fluids in the metamorphism of komatiites, Agnew nickel deposit, Western Australia. *Contributions to Mineralogy and Petrology* **96**, 151–162.

Groves, D. I., Barrett, F. M., Binns, R. A. & McQueen, K. G. (1977). Spinel phases associated with metamorphosed volcanic-type iron–nickel sulfide ores from Western Australia. *Economic Geology* **72**, 1224–1244.

Hoffman, M. A. & Walker, D. (1978). Textural and chemical variations of olivine and chromite spinel in the East Dover ultramafic bodies, south–central Vermont. *Geological Society of America Bulletin* **89**, 699–710.

Irvine, T. N. (1965). Chromian spinel as a petrogenetic indicator. Part I. Theory. *Canadian Journal of Earth Sciences* **2**, 648–672.

Jackson, E. D. (1966). Chemical variation in coexisting chromite and olivine in chromitite zones of the Stillwater Complex. *Economic Geology* **61**, 794.

Johannes, W. (1969). An experimental investigation of the system $MgO–SiO_2–H_2O–CO_2$. *American Journal of Science* **267**, 1083–1104.

Kimball, K. L. (1990). Effects of hydrothermal alteration on the compositions of chromian spinels. *Contributions to Mineralogy and Petrology* **105**, 337–346.

Lesher, C. M., Arndt, N. T. & Groves, D. I. (1984). Genesis of komatiite-associated nickel sulphide deposits at Kambalda, Western Australia: a distal volcanic model. In: Buchanan, D. L. & Jones, M. J. (eds) *Sulphide Deposits in Mafic and Ultramafic Rocks*. London: Institute of Mining and Metallurgy, pp. 70–80.

Loferski, P. J. & Lipin, B. R. (1983). Exsolution in metamorphosed chromite from the Red Lodge district, Montana. *American Mineralogist* **68**, 777–789.

McQueen, K. G. (1979). Metamorphism and deformation of volcanic associated nickel deposits: a study of mineralization around the Widgiemooltha Dome, Western Australia. Ph.D. thesis. University of Western Australia: Nedlands, Western Australia.

McQueen, K. G. (1981). The nature and metamorphic history of the Wannaway nickel deposit, Western Australia. *Economic Geology* **76**, 1444–1468.

Onyeagocha, A. C. (1974). Alteration of chromite from the Twin Sisters dunite, Washington. *American Mineralogist* **59**, 608–612.

Parker, P. (1984). The role of contamination in the formation of the nickel sulphide ores at Wannaway and Mt. Edwards, Western Australia. Honours Thesis, B.Sc. thesis. University of Western Australia: Nedlands, Western Australia, 144 pp.

Robinson, B. W. & Graham, J. (1992). Advances in electron microprobe trace-element analysis. *Journal of Computer-Assisted Microscopy* **4**, 263–265.

Roeder, P. L., Campbell, I. H. & Jamieson, H. E. (1979). Re-evaluation of the olivine–spinel geothermometer. *Contributions to Mineralogy and Petrology* **68**, 325–334.

Sack, R. O. & Ghiorso, M. S. (1991). Chromian spinels as petrogenetic indicators: thermodynamic and petrological applications. *American Mineralogist* **76**, 827–847.

Ulmer, G. C. (1974). Alteration of chromite during serpentinization in the Pennsylvania–Maryland District. *American Mineralogist* **59**, 1236–1241.

Ware, N. G. (1981). Computer programs and calibration with the PIBS technique for quantitative electron probe analysis using a lithium-drifted silicon detector. *Computers and Geosciences* **7**, 167–184.

Ware, N. G., Robinson, B. W. & Walker, R. K. (1988). Programming for microprocessor operated instrumentation. *Proceedings of AXAA-88, Australian X-Ray Analysis Conference, Perth, W.A., 1998*. Perth: Australian X-ray Analytical Association, pp. 509–513.

Will, T. M., Powell, R. & Holland, T. J. B. (1990). A calculated petrogenetic grid for ultramafic rocks in the system $CaO–FeO–MgO–Al_2O_3–SiO_2–CO_2–H_2O$. *Contributions to Mineralogy and Petrology* **105**, 347–358.

Wylie, A. G., Candela, P. A. & Burke, T. M. (1987). Compositional zoning in unusual Zn-rich chromite from the Sykesville district of Maryland and its bearing on the origin of the 'ferritchromit'. *American Mineralogist* **72**, 413–422.

Zhou, M.-F. & Kerrich, R. (1992). Morphology and composition of chromite in komatiites from the Belingwe Greenstone Belt, Zimbabwe. *Canadian Mineralogist* **30**, 303–317.

APPENDIX A: DATA SOURCES

Table A1: Sources of data used in this paper

Locality	Data source	Metm. grade	Chromite points	Samples analysed
Norseman–Wiluna Belt				
Black Swan	This study	G	87	8
Honeymoon Well	Donaldson (1981)	G	5	5
Honeymoon Well	This study	G	72	9
Kambalda	Frost & Groves (1989)	A	5	4
Kambalda	Donaldson (1981)	A	6	6
Kambalda	This study	A	261	23
Marshall Pool	Donaldson (1981)	G	6	6
Mt Clifford–Marshall Pool	This study	G	174	13
Mt Keith	This study	G	792	51
Perseverance	Barnes *et al.* (1993)	A	39	8
Perseverance	This study	A	159	10
Scotia	This study	G	71	4
Walter Williams	Gole & Hill (1990)	G	102	75
Walter Williams	This study	G	91	7
Widgiemooltha	Parker (1984)	A	295	
Yakabindie	Donaldson (1981)	G	16	15
Other localities (literature data)				
Munro and Beatty Twps, Abitibi Belt	Allen (1990) Arndt *et al.* (1977)	G	31	
Belingwe Belt	Zhou & Kerrich (1992)	G	98	
Kuhmo Belt, Finland	Blais & Auvray (1990)	A	16	
Total			2326	245

APPENDIX B: LOCALITY DESCRIPTIONS

The following brief descriptions summarize the rock types and dominant metamorphic mineralogy of the samples represented in this study.

Black Swan. A 500 m thick by 2·5 km long complex of mainly olivine orthocumulate rocks, metamorphosed at lowermost greenschist facies (Barnes & Hill, 2000). Metamorphic assemblages dominated by talc–carbonate ± quartz rocks, with minor antigorite–carbonate and lizardite serpentinites.

Honeymoon Well. Olivine adcumulates and mesocumulates, lower greenschist facies lizardite serpentinites with stichtite, no fresh olivine (Gole & Hill, 1990).

Kambalda. Dominantly olivine orthocumulate to mesocumulate rocks, talc–carbonate assemblages formed at lower amphibolite facies conditions (Archibald *et al.*, 1978).

Marshall Pool and Mt Clifford. Olivine adcumulates, lizardite serpentinites with local preservation of fresh olivine, lower greenschist facies.

Mt Keith. Spectrum of lithologies from olivine adcumulates to spinifex-textured komatiite flows, mainly lizardite serpentines with stichtite, with lesser antigorite–carbonate serpentinites. Lower to mid-greenschist facies.

Perseverance. Olivine meso- to adcumulates, lower amphibolite facies rocks with metamorphic olivine plus talc, anthophyllite and locally enstatite (Gole *et al.*, 1987), and variable degrees of retrogressive serpentinization of metamorphic olivine.

Scotia. Olivine mesocumulates, antigorite serpentinites with abundant relic fresh olivine, upper greenschist facies.

Walter Williams. Olivine ortho-, meso- and adcumulates, mainly lizardite serpentinites with locally abundant fresh olivine, lower to upper greenschist.

Widgiemooltha. Olivine ortho- to mesocumulates, mixture of talc–carbonates and metamorphic olivine–tremolite–chlorite lithologies, lower to mid-amphibolite facies (Archibald *et al.*, 1978).

APPENDIX C: ANALYTICAL METHODS AND RESULTS

All elements were analysed by wavelength-dispersive electron microprobe analysis using standard procedures on the Cameca SX50 instrument at CSIRO Exploration and Mining, Floreat Park, Western Australia. The elements Si, Ti, Al, Fe, Mg, Mn, Ca and Zn were analysed under the following conditions: accelerating voltage 30 kV, beam current 30 nA, using stepwise peak integration and background stripping, with online ZAF correction procedures (Ware, 1981; Ware *et al.*, 1988). The major elements were counted for 20 s, and minor elements Ti, Mn and Zn for 80 s each. 'Trace' elements Ni, Co and V were analysed using the 'CSIROTrace' procedure (Robinson & Graham, 1992), under conditions of 30 kV accelerating voltage and 450 nA, with count times of 50–100 s, and offline ZAF correction. Other details of methods and standards have been reported by Barnes (1998). Summarized average analyses of chromite cores are reported in Table C1. Full analytical data are available from the author on request.

Table C1: Summarized average analyses of chromite cores and magnetite rims for samples analysed in this study

Sample	Phase	Analyses	SiO_2	TiO_2	V_2O_5	Al_2O_3	Cr_2O_3	Fe_2O_3	FeO	MnO	MgO	CoO	NiO	ZnO	Total	Cr/ Σ^{3+} ions	Al/ Σ^{3+} ions	Fe^{3+}/ Σ^{3+} ions	Mg/ $(Mg+Fe^{2+})$	Cr/ (Cr+Al)
Kambalda																				
KD0262-1031.2	chromite	6	0·13	0·25	0·12	10·17	51·81	6·14	27·97	0·79	0·70	0·04	0·02	2·46	100·60	0·71	0·21	0·08	0·04	0·77
KD0262-1031.2	magnetite	3	0·04	0·03	0·41	0·02	3·84	65·91	28·53	0·02	0·04	0·00	0·04	0·00	98·87	0·04	0·00	0·96	0·00	0·99
KD0262-1067.6	chromite	14	0·10	0·26	0·14	10·78	51·51	5·88	28·12	0·83	1·05	0·07	0·03	1·86	100·62	0·70	0·22	0·08	0·06	0·76
KD0262-1067.6	magnetite	3	0·26	0·07	0·20	0·09	13·58	57·59	27·46	0·23	0·15	0·01	0·06	0·18	99·88	0·15	0·00	0·85	0·01	0·99
KD0262-1106.3	chromite	8	0·10	0·22	0·13	10·08	51·32	6·07	26·05	1·15	0·75	0·04	0·03	3·76	99·69	0·71	0·21	0·08	0·04	0·77
KD0262-1106.3	magnetite	7	0·02	0·05	0·45	0·03	3·59	66·64	28·78	0·06	0·03	0·00	0·08	0·04	99·77	0·04	0·00	0·96	0·00	0·99
KD0272-0696.0	chromite	9	0·13	0·21	0·10	9·86	52·74	4·71	28·58	0·44	0·86	0·07	0·02	1·87	99·59	0·73	0·20	0·06	0·05	0·78
KD0272-0696.0	magnetite	7	0·41	0·04	0·27	0·11	11·31	58·51	27·19	0·09	0·27	0·01	0·07	0·21	98·50	0·13	0·00	0·87	0·01	0·99
KD0272-0723.0	chromite	9	0·12	0·21	0·12	9·56	53·24	5·21	29·31	0·61	0·63	0·02	0·02	1·42	100·47	0·73	0·20	0·07	0·03	0·79
KD0272-0723.0	magnetite	9	0·05	0·03	0·43	0·06	10·05	61·21	28·49	0·06	0·03	0·00	0·07	0·10	100·58	0·11	0·00	0·89	0·00	0·99
KD0272-0793.3	chromite	7	0·11	0·21	0·09	10·35	52·04	5·34	28·97	0·66	0·73	0·04	0·03	1·46	100·02	0·72	0·21	0·07	0·04	0·77
KD0272-0793.3	magnetite	3	0·28	0·01	0·37	0·14	11·53	58·55	27·60	0·10	0·12	0·01	0·09	0·15	98·96	0·13	0·00	0·87	0·01	0·99
KD0272-0868.1	chromite	6	0·10	0·22	0·10	10·80	52·49	4·75	28·93	0·24	1·39	0·08	0·03	1·64	100·75	0·72	0·22	0·06	0·07	0·77
KD0272-0868.1	magnetite	5	0·04	0·02	0·23	0·01	5·10	65·62	28·32	0·01	0·06	0·00	0·22	0·03	99·66	0·05	0·00	0·94	0·00	1·00
KD0272-0928.1	chromite	15	0·12	0·24	0·15	10·57	52·70	5·00	28·25	1·05	0·95	0·04	0·06	2·02	101·14	0·72	0·21	0·06	0·05	0·77
KD0272-0928.1	magnetite	17	0·06	0·06	0·36	0·02	1·51	68·50	28·78	0·02	0·06	0·00	0·05	0·01	99·42	0·02	0·00	0·98	0·00	0·98
KD0272-1177.5	chromite	4	0·12	0·22	0·11	11·00	52·74	4·84	26·65	0·26	1·59	0·06	0·03	3·76	101·36	0·71	0·22	0·06	0·09	0·76
KD0272-1177.5	magnetite	4	0·04	0·06	0·48	0·00	1·38	68·78	29·06	0·00	0·06	0·00	0·12	0·01	99·99	0·01	0·00	0·98	0·00	1·00
KD0275-620·11	chromite	6	0·11	0·21	0·10	10·14	52·51	5·34	28·12	0·38	0·91	0·12	0·01	2·86	100·81	0·72	0·21	0·07	0·05	0·78
KD0275-620·11	magnetite	6	0·04	0·00	0·26	0·01	4·19	66·92	28·64	0·00	0·04	0·01	0·19	0·05	100·35	0·04	0·00	0·95	0·00	1·00
KD0275-650.7	chromite	9	0·12	0·23	0·13	10·47	52·76	4·53	29·41	0·54	0·92	0·09	0·04	1·20	100·44	0·72	0·21	0·06	0·05	0·77
KD0275-650.7	magnetite	11	0·05	0·01	0·35	0·01	3·42	66·45	28·43	0·00	0·03	0·00	0·15	0·02	98·92	0·04	0·00	0·96	0·00	1·00
KD0275-786.1	chromite	7	0·12	0·23	0·12	10·87	52·15	4·57	28·50	0·46	0·93	0·05	0·02	2·36	100·37	0·72	0·22	0·06	0·05	0·76
KD0283-409.7	chromite	38	0·15	0·23	0·07	10·19	52·74	4·60	25·72	1·24	0·91	0·01	0·06	4·38	100·32	0·73	0·21	0·06	0·05	0·78
KD0283-409.7	magnetite	14	0·41	0·10	0·32	0·15	8·51	61·08	27·37	0·24	0·32	0·00	0·02	0·32	98·84	0·09	0·00	0·90	0·01	0·98
KD0283-431.7	magnetite	5	0·21	0·04	0·22	0·06	8·83	61·15	27·55	0·04	0·21	0·01	0·06	0·09	98·47	0·10	0·00	0·90	0·01	0·99
KD1236-496.3	chromite	12	0·10	0·24	0·18	13·06	48·10	6·64	28·51	0·49	0·46	0·07	0·01	3·46	101·30	0·65	0·26	0·08	0·03	0·71

Table C1: continued

Sample	Phase	Analyses	SiO_2	TiO_2	V_2O_5	Al_2O_3	Cr_2O_3	Fe_2O_3	FeO	MnO	MgO	CoO	NiO	ZnO	Total	Cr/ Σ^{3+} ions	Al/ Σ^{3+} ions	Fe^{3+}/ Σ^{3+} ions	Mg/ (Mg+Fe^{2+})	Cr/ (Cr+Al)
Kambalda																				
KD1236-496.3	magnetite	14	0·06	0·02	0·30	0·08	5·00	65·96	28·66	0·05	0·02	0·01	0·04	0·10	100·29	0·05	0·00	0·94	0·00	0·99
KD1236-541.07	chromite	4	0·14	0·20	0·08	9·88	51·89	5·39	28·62	0·69	0·61	0·04	0·01	1·61	99·15	0·72	0·21	0·07	0·03	0·78
KD1236-541.07	magnetite	2	0·05	0·00	0·28	0·01	4·01	66·12	28·39	0·00	0·04	0·00	0·08	0·00	98·98	0·04	0·00	0·96	0·00	1·00
KD1236-594.0	chromite	5	0·12	0·22	0·10	9·99	52·79	5·70	29·82	0·47	0·83	0·04	0·03	1·12	101·23	0·72	0·20	0·07	0·04	0·78
KD1236-594.0	magnetite	3	0·34	0·05	0·48	0·09	10·26	59·54	28·52	0·10	0·22	0·00	0·03	0·07	99·68	0·11	0·00	0·88	0·01	0·99
KD1236-614.3	chromite	13	0·13	0·21	0·10	10·06	53·31	5·46	29·35	0·24	1·46	0·10	0·03	0·47	100·91	0·72	0·20	0·07	0·08	0·78
KD1236-614.3	magnetite	5	0·13	0·04	0·33	0·09	11·86	59·64	28·06	0·03	0·17	0·01	0·25	0·00	100·61	0·13	0·00	0·87	0·01	0·99
KD1236-642.1	chromite	20	0·11	0·21	0·12	9·98	51·43	7·49	28·36	0·27	1·55	0·19	0·06	1·12	100·90	0·70	0·20	0·10	0·08	0·78
KD1236-642.1	magnetite	9	0·05	0·03	0·17	0·07	13·46	57·44	28·04	0·04	0·06	0·06	0·40	0·11	99·94	0·15	0·00	0·85	0·00	0·99
KD1236-669.3	chromite	22	0·13	0·19	0·14	9·77	50·55	8·19	26·30	1·22	1·27	0·19	0·05	2·22	100·23	0·69	0·20	0·11	0·07	0·78
KD1236-669.3	magnetite	6	0·18	0·00	0·19	0·02	6·62	64·00	27·73	0·06	0·10	0·01	0·63	0·06	99·60	0·07	0·00	0·93	0·00	1·00
KD1236-687.2	chromite	5	0·09	0·24	0·17	11·49	51·49	5·80	28·74	0·30	1·53	0·17	0·04	1·25	101·30	0·69	0·23	0·07	0·08	0·75
KD1236-687.2	magnetite	5	0·01	0·00	0·22	0·00	4·15	66·65	28·33	0·00	0·03	0·00	0·50	0·01	99·90	0·04	0·00	0·95	0·00	1·00
KD1236-695.7	chromite	7	0·10	0·23	0·13	11·45	52·30	4·59	28·70	0·32	1·67	0·10	0·02	1·31	100·93	0·71	0·23	0·06	0·09	0·75
KD1236-695.7	magnetite	5	0·04	0·00	0·22	0·00	4·59	65·67	27·96	0·01	0·05	0·00	0·66	0·00	99·21	0·05	0·00	0·95	0·00	1·00
Mt Goode																				
MGD22C-578	chromite	10	0·13	0·26	0·08	4·53	46·88	19·90	21·42	0·95	4·66	0·08	0·14	1·75	100·77	0·61	0·09	0·29	0·23	0·89
MGD22C-578	magnetite	29	0·20	0·28	0·08	0·05	22·09	49·76	24·26	0·67	2·73	0·04	0·58	0·43	101·16	0·24	0·00	0·75	0·11	1·00
MGD22D-33.2	chromite	13	0·21	0·36	0·19	6·48	48·90	15·38	24·06	0·70	3·58	0·10	0·15	1·01	101·12	0·65	0·13	0·22	0·18	0·84
MGD22D-33.2	magnetite	29	0·16	1·45	0·38	0·12	19·43	50·96	26·54	0·55	1·27	0·05	0·71	0·19	101·82	0·22	0·00	0·76	0·05	0·99
Perseverance																				
LSD191-138.9	chromite	9	0·00	0·28	0·19	11·97	51·32	6·07	24·02	0·75	4·01	0·03	0·02	1·75	100·41	0·68	0·24	0·08	0·21	0·74
WAM24-279.65	chromite	6	0·00	0·68	0·22	6·03	47·30	17·92	23·88	0·68	3·42	0·05	0·04	0·92	101·14	0·61	0·12	0·26	0·17	0·86
WAP071-1682	chromite	3		0·29	0·09	11·30	52·33	5·45	21·39	1·78	5·35			2·60	100·57	0·70	0·23	0·07	0·29	0·76
WAP079-183.6	chromite	2		0·31	0·13	9·78	52·95	6·91	24·31	1·02	3·82			1·63	100·83	0·71	0·20	0·09	0·20	0·78
WAP079-410	chromite	14		0·40	0·12	6·35	51·43	14·31	20·82	0·63	5·44			1·11	100·60	0·67	0·12	0·20	0·27	0·85
WAP104-560	chromite	4		0·27	0·12	12·06	51·86	6·19	22·87	0·59	5·69			1·05	100·69	0·69	0·23	0·08	0·29	0·75
WAP104-896	chromite	7		0·25	0·10	8·41	53·70	8·25	23·88	1·35	3·97			1·36	101·27	0·72	0·17	0·11	0·21	0·81
WAP79-1682	chromite	7	0·00	0·24	0·12	10·41	51·34	9·94	19·95	1·80	5·36	0·07	0·02	2·28	101·52	0·67	0·20	0·13	0·28	0·77

Sample	Phase	Analyses	SiO_2	TiO_2	V_2O_5	Al_2O_3	Cr_2O_3	Fe_2O_3	FeO	MnO	MgO	CoO	NiO	ZnO	Total	Cr/ Σ^{3+} ions	Al/ Σ^{3+} ions	Fe^{3+}/ Σ^{3+} ions	Mg/ $(Mg+Fe^{2+})$	Cr/ $(Cr+Al)$
Perseverance																				
WAP79-410	chromite	4	0·00	0·22	0·14	8·27	51·83	12·51	20·64	0·50	5·95	0·09	0·04	1·01	101·19	0·67	0·16	0·17	0·29	0·81
WAP84-723	chromite	2		0·29	0·16	8·80	54·91	7·51	22·02	1·05	5·57			1·07	101·36	0·73	0·17	0·10	0·28	0·81
WAP84-723	magnetite	1		0·42	0·10	0·03	10·99	61·18	26·89	0·38	1·01			0·17	101·17	0·12	0·00	0·88	0·04	1·00
WAT09-183.6	chromite	1		0·30	0·14	9·69	52·53	7·55	24·23	1·01	3·86			1·82	101·14	0·71	0·19	0·10	0·20	0·79
WAT10-158.10	chromite	27	0·07	0·30	0·17	7·19	51·73	12·67	20·53	0·76	5·39	0·07	0·06	0·97	99·90	0·68	0·14	0·18	0·28	0·84
WAT9-183.6	chromite	8	0·00	0·28	0·15	9·78	51·36	9·65	23·55	0·94	3·82	0·07	0·03	1·58	101·19	0·68	0·19	0·13	0·20	0·78
WPU332-269	chromite	13	0·14	1·02	0·48	2·43	44·64	23·55	24·25	0·70	1·74	0·02	0·14	0·80	99·90	0·59	0·05	0·35	0·09	0·93
WPU332-269	magnetite	1	0·00	0·61	0·17	0·17	36·55	36·10	22·64	0·87	2·68	0·05	0·23	0·42	100·49	0·44	0·00	0·55	0·13	0·99
WPU469-39.10	magnetite	8	0·04	1·70	0·23	0·14	15·21	54·68	26·24	0·59	1·03	0·01	0·14	0·14	100·15	0·17	0·00	0·80	0·04	0·99
WPU469-39.8	magnetite	1	0·00	1·55	0·19	0·11	12·46	57·10	26·33	0·55	0·96	0·01	0·13	0·12	99·52	0·14	0·00	0·84	0·04	0·99
WPU469-39.9	magnetite	1	0·00	2·10	0·27	0·20	20·32	49·23	25·58	0·56	1·34	0·02	0·19	0·21	100·02	0·24	0·00	0·73	0·06	0·99
WPU469-40.8	chromite	67	0·03	0·36	0·13	2·90	56·45	11·27	23·29	1·28	2·70	0·03	0·03	1·19	99·65	0·78	0·06	0·16	0·15	0·93
WPU469-40.8	magnetite	50	0·14	1·32	0·13	0·37	27·42	43·11	24·16	1·03	1·76	0·01	0·09	0·35	99·89	0·33	0·01	0·65	0·08	0·98
Scotia																				
23245	chromite	21	0·10	0·25	0·12	10·92	53·57	5·85	23·75	0·50	4·82	0·08	0·12	0·74	100·82	0·71	0·21	0·07	0·24	0·77
23246	chromite	7	0·12	0·30	0·14	12·16	50·85	6·61	24·48	0·52	4·14	0·10	0·08	1·00	100·50	0·67	0·24	0·08	0·21	0·74
23247	chromite	18	0·10	0·26	0·14	11·47	52·17	5·51	24·30	0·46	4·28	0·08	0·10	0·95	99·82	0·70	0·23	0·07	0·22	0·75
23248	chromite	25	0·19	0·27	0·16	11·99	51·16	5·89	22·62	0·52	5·19	0·11	0·10	0·94	99·14	0·68	0·24	0·08	0·27	0·74
23248	magnetite	12	0·04	0·31	0·15	0·04	13·17	58·40	27·29	0·19	0·56	0·06	0·40	0·09	100·70	0·15	0·00	0·85	0·02	1·00
Windarra																				
86228	chromite	12	0·12	0·19	0·12	9·46	51·76	8·37	25·21	1·04	1·71	0·06	0·01	2·93	100·98	0·69	0·19	0·11	0·10	0·79
86228	magnetite	9	0·05	0·08	0·24	0·05	17·08	54·80	27·61	0·32	0·15	0·01	0·09	0·29	100·78	0·19	0·00	0·81	0·01	1·00
86230	chromite	18	0·12	0·19	0·12	10·15	52·27	6·35	24·77	1·17	1·69	0·06	0·01	4·10	100·99	0·71	0·20	0·08	0·10	0·78
86230	magnetite	10	0·04	0·07	0·23	0·08	16·77	54·57	27·32	0·43	0·15	0·01	0·07	0·41	100·15	0·18	0·00	0·81	0·01	0·99
GE280-633.5	chromite	12	0·12	0·23	0·17	9·01	49·63	10·82	24·85	0·79	0·98	0·07	0·01	4·10	100·78	0·67	0·18	0·15	0·06	0·79
GE280-633.5	magnetite	10	5·30	0·07	0·28	0·10	14·29	53·19	24·24	0·25	2·72	0·01	0·08	0·47	100·99	0·16	0·00	0·84	0·16	0·97
PSD11-995	chromite	28	0·13	0·23	0·21	7·90	50·55	11·27	24·66	1·44	1·09	0·06	0·01	3·13	100·68	0·68	0·16	0·16	0·06	0·82
PSD11-995	magnetite	25	0·02	0·09	0·21	0·10	15·44	57·00	27·29	0·40	0·13	0·01	0·10	0·44	101·22	0·17	0·00	0·82	0·01	0·99